CZECH TECHNICAL UNIVERSITY IN PRAGUE

FACULTY OF MECHANICAL ENGINEERING

DEPARTMENT OF INSTRUMENTATION AND CONTROL ENGINEERING

SENSOR FOR PCB WARPING MEASUREMENT

BACHELOR THESIS

2021 **Dingyuan Yao**

BACHELOR'S THESIS ASSIGNMENT

I. Personal and study details

Student's name: **Yao Dingyuan** Personal ID number: **472246**

Faculty / Institute: **Faculty of Mechanical Engineering**

Department / Institute: **Department of Instrumentation and Control Engineering**

Study program: **Bachelor of Mechanical Engineering**

Branch of study: **Information and Automation Technology**

II. Bachelor's thesis details

Bachelor's thesis title in English:

Sensor for PCB warping measurement

Bachelor's thesis title in Czech:

Senzor pro měření deformace desky plošných spojů

Guidelines:

- Research of methods of measuring small deformations.
- Choosing a system suitable for the measurement of a PCB warping during the soldering process, considering the enviromental conditions (high temperature, restricted space).
- Analysis of the method's sensitivity, robustness, tolerance to temperature changes.
- Design of a proof-of-concept setup.

Bibliography / sources:

[1] Krohn, David A., MacDougall, Trevor W. and Mendez, Alexis. Fiber Optic Sensors: Fundamentals and Applications, Fourth Edition. Bellingham, WA : SPIE PRESS BOOK, 2015. ISBN: 9781628411805.
[2] T. Li, Chaoyang Shi, H. Ren. A Novel Fiber Bragg Grating Displacement Sensor With a Sub-Micrometer Resolution. DOI:10.1109/LPT.2017.2712602.
[3] E. Derniak: Geometrical and Trigonometric Optics, Cambridge 2008

Name and workplace of bachelor's thesis supervisor:

Ing. Bc. Šárka Němcová, Ph.D., Division of Precision Mechanics and Optics, FME

Name and workplace of second bachelor's thesis supervisor or consultant:

Date of bachelor's thesis assignment: **30.04.2021** Deadline for bachelor thesis submission: **10.06.2021**

Assignment valid until: _____

Ing. Bc. Šárka Němcová, Ph.D. Supervisor's signature	Head of department's signature	prof. Ing. Michael Valášek, DrSc. Dean's signature

III. Assignment receipt

The student acknowledges that the bachelor's thesis is an individual work. The student must produce his thesis without the assistance of others, with the exception of provided consultations. Within the bachelor's thesis, the author must state the names of consultants and include a list of references.

Date of assignment receipt	Student's signature

Statement

I declare that I have worked out this thesis independently assuming that the results of the thesis can also be used at the discretion of the supervisor of the thesis as its co-author. I also agree with the potential publication of the results of the thesis or of its substantial part, provided I will be listed as the co-author.

Prague 10.08.2021 Signature 

Abstract

This thesis presents a method for PCB warpage detection based on fiber optic displacement sensors, based on the traditional method of measuring PCB warpage with a marble measuring table. At the same time, the article also describes lots of other optical displacement sensors, including their working principles, measurement accuracy, working environment, etc. At the end of the subject, a chromatic confocal sensor will be designed individually using two ready-made lenses.

Keywords: PCB warping, optical measurement, fiber optical sensor, chromatic confocal sensor.

.

Table of content

Chapter 1. Introduction

1.1 Research background

In recent years, the thermal-mechanical reliability of microelectronic devices has become increasingly important as microelectronic packages move towards lighter, smaller and more highly integrated devices. The mismatch in thermal expansion coefficients of various packaging materials in microelectronic devices during manufacture and use can lead to many reliability problems such as warpage and deformation of the substrate. The warpage of printed circuit boards (PCB substrates), ceramic substrates, silicon substrates and metal substrates during the packaging process is one of the most important factors affecting the quality, performance and reliability of microelectronic devices. This also brings a lot of misfortune to PCB manufacturers and assemblers, such as loss of profit due to rework, breakage and component damage. Therefore, in order to improve the reliability and yield of microelectronic devices, it is essential to measure the warpage of the device substrate during the package manufacturing process.

The rapid development of the electronics industry and the widespread use of SMT (surface-mount technology) automated insertion equipment and placement equipment are placing increasingly high demands on the quality of printed boards. Nowadays, with the emergence of HDI (High Density Interconnector) boards and IC (integrated circuit) carrier boards, as well as the application of vast SMD (surface-mount device) components and IC chips, this has more stringent requirements for the warpage of printed boards. If the board leveling does not meet the requirements, will seriously affect the finished board qualification rate, resulting in a mass of subsequent false welding, leakage of solder and the inability to weld the situation, and ultimately will seriously affect the use of electronic products performance [1].

1.2 Traditional warpage measurement methods

At present, most circuit board manufacturers use marble measuring tables to measure board warpage. The printed board is placed flat on the marble measuring table, and the four corners of the board are gently tapped by hand to determine whether the board is warped, and then the specific data of the board warpage is measured by a "plug gauge" [2]. This measurement method of manual judgement of board warpage has a higher chance of missing detection, different personnel measure the data differently and the measurement is not efficient. Defined respectively as follows [3]:

(1) Maximum percentage of bow = bow maximum vertical displacement (D) / length of the maximum vertical displacement (L) × 100%, figure 1.2.

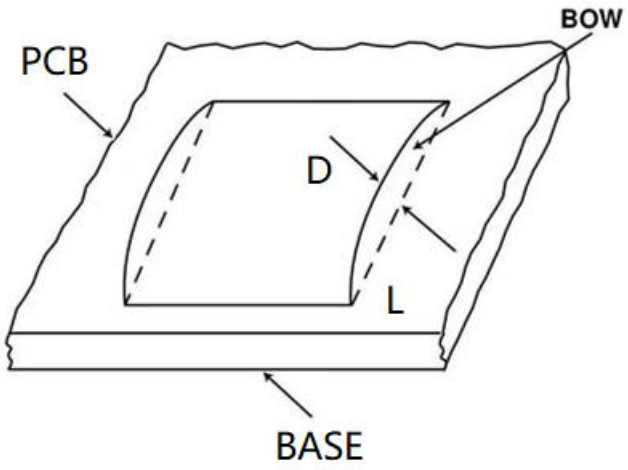

figure 1.2

(2) Maximum percentage of twist = maximum vertical displacement of twist (D) / diagonal length of sample tested (L) x 100%, figure 1.3.

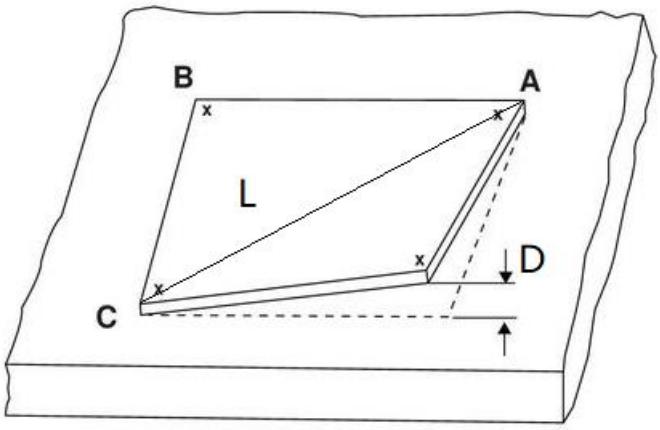

figure 1.3

The Bow and Twist is the unintended change in the geometry of a PCB that determines the level of flatness in a circuit board. Board warpage is a common term used to describe altered shape of PCB, which can either be a Bow or a Twist.

A Bow is a condition in a PCB where all 4 corners more or less stay in the same plane, but the board material displays cylindrical or spherical curvature.

A Twist is the board deformation parallel to the diagonal of the board such that one or both diagonal corners are not in the same plane compared to the remaining corners that normally stay flat.

According to the IPC standard [4], the board warpage is usually less than 0.75%, which means that the board is qualified. Some manufacturers have higher warpage requirements for copper clad boards and circuit boards, with board warpage requirements less than or equal to 0.3 percent. When the PCB board warpage can not meet the requirements, will seriously affect the SMT assembly of the welding quality,

resulting in vast of substandard products.

1.3 Optical measurement

The development of traditional contact measurement methods has been very mature, with high reliability and stability, but there is contact pressure between the measuring head and the measured object during measurement, which is easy to damage the surface of the measured object. Especially in the microelectronic packaging industry, the surface of the sample to be tested is generally very finely structured, and the contact measurement method will destroy the sample. In addition, the contact measurement is performed in a point-by-point manner, and the measurement efficiency is low.

Non-contact measurement methods mainly include optical measurement methods. In recent years, optical measurement methods have developed rapidly and have begun to be widely used in more and more fields. The non-contact optical measurement method is one of the most widely used three-dimensional measurement methods due to its high measurement efficiency, non-destructive, easy to achieve full-field measurement and other advantages.

1.4 Research content

The article focuses on the measurement of PCB warpage proposing a more precise non-contact measurement method based on the traditional contact measurement. The measurement system is built for the color confocal measurement method. The main work to be carried out in the thesis includes the following parts:

(1) Introduce what is a PCB, why warping occurs and the hazards of warping. Analyze the traditional contact measurement, put forward the shortcomings and lead to the non-contact measurement method.

(2) Introduce various non-contact optical displacement sensors, such as triangular displacement sensors, interferometric measurement methods, capacitive displacement sensors, etc. Compare various displacement sensor parameters such as measuring range, accuracy, etc. Screen suitable displacement sensors according to the conditions required by the experiment.

(3) Focus on the working principle of the chromatic confocal measurement method. Design and build a chromatic confocal sensor system.

(4) Conduct experiments and statistics

(5) Analyze and summarize the data obtained from the experiment.

Chapter 2. Noncontact optical sensing techniques

Introduced the principle, classification and characteristics of displacement sensors, fiber optic sensors, and fiber optic displacement sensors.

2.1 Displacement sensors

Displacement sensors, also known as linear sensors, include inductive displacement sensors, capacitive displacement sensors, photoelectric displacement

sensors, and ultrasonic displacement sensors. They are one of the most widely used sensors.[5]

2.2 Eddy Current displacement sensors

2.2.1 Eddy current effect

The plane of the loop is perpendicular to the direction of the magnetic field. Figure 2.1 shows the common generation of eddy currents, which correspond to alternating magnetic fields and relative moving magnetic fields, respectively.

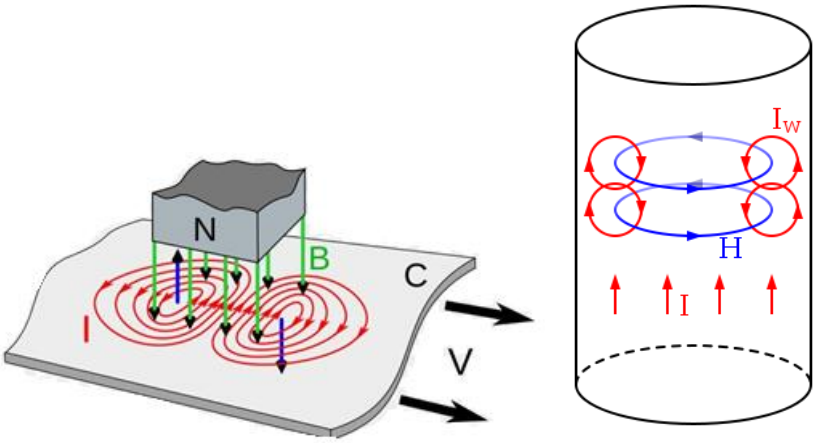

Figure 2.1 Two forms of eddy current generation [6].

C is the metal sheet.
B is the magnetic field.
I is eddy current.
N is the magnet's north pole.
V is the moving velocity of the metal sheet.
H is the magnetic field intensity.

The vortex effect has three external manifestations:

(1) Mutual inductance effect: the eddy current magnetic field has an offsetting effect on the original magnetic field of the coil

(2) Thermal effect: vortex will lose energy and generate heat

(3) Force effect: the electromagnetic force produced by the eddy current magnetic field and the original magnetic field is shown as resistance

2.2.2 Working principle of eddy current sensor

The eddy current sensor is composed of a detection coil (probe), a target conductor, and a signal processing circuit. When an alternating current flows through the coil, the coil magnetic field will excite eddy currents in the nearby metal, and the alternating magnetic field of the eddy current is opposite to the magnetic field of the coil. Because the eddy current magnetic field has a counteracting effect on the original magnetic field, the equivalent inductance of the coil is reduced; at the same time, the eddy current itself consumes energy, which causes the equivalent resistance

to increase. If the metal material is a magnetically permeable material, the effect on the magnetic flux after the metal plate is magnetized must be considered. The equivalent impedance of the detection coil can be written as [7]:

$$Z_{eff} = f(x, \mu, d, f, \rho)$$

Among them, ρ is the resistivity of the metal conductor, μ is the magnetic permeability, d is the thickness of the conductor, and f is the excitation frequency. When the value x (the displacement) in the equation is changed and other variables μ, d, f, ρ are fixed, this displacement x can be reflected by measuring the change of Z_{eff}, and the eddy current sensor can measure displacement by slightly changing the form.

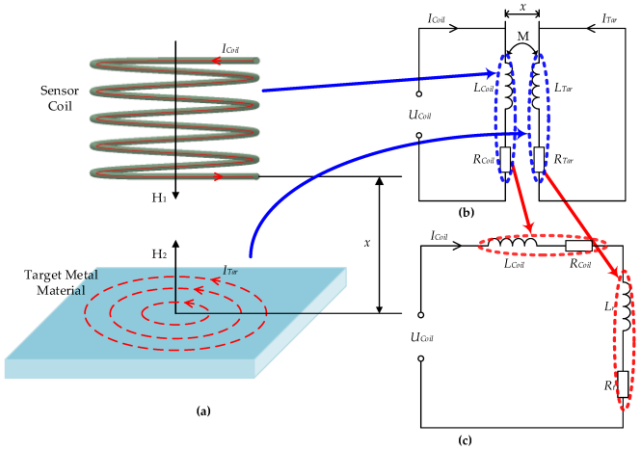

Figure 2.2 Principle of displacement measurement based on eddy current displacement sensor (ECDS): (a) principle model; (b) simplified circuit; (c) equivalent circuit [8].

For my opinion: eddy current sensor has good measuring range, resolution and suitable size. For example, eddyNCDT 3060-ES-U1, it has 1mm measuring range, 0.02μm resolution and maximum 10mm diameter link for the sensor: https://www.micro-epsilon.com/download/products/cat--eddyNCDT--en.pdf. However, eddy current sensor requires the participation of the circuit part. The resistance value of the internal resistor will change at a high temperature of 250℃, and the resistance efficiency will also decrease, so the operating temperature of most of these sensors on the market is within 70℃. After adding high temperature resistant materials, the temperature that the eddy current sensor can withstand will increase. But there is still no such sensor that can meet the high temperature of 250℃, eddy current sensor cannot be used in this experiment.

2.3 Capacitive displacement sensor

Capacitive displacement sensor is a sensor that uses a capacitor as a sensitive element to convert mechanical displacement into a change in capacitance.

2.3.1 Working principle of capacitive displacement sensor

Capacitive displacement sensors operate by measuring changes in capacitance. Capacitance describes how there is a gap between two conductive objects in response

to the voltage difference applied to them. When a voltage is applied to a conductor, an electric field is generated between the conductors, which accumulates positive and negative charges on each object. Capacitive sensors use AC voltage, which causes the charge to constantly reverse its position. This generates alternating current that is detected by the sensor. The capacitance is proportional to the surface area of the object and the dielectric constant of the material between the objects, and inversely proportional to the distance between the objects.

The principle of capacitance displacement measurement is based on the working principle of an ideal plate-type capacitor. The distance displacement of the plate (sensor and measurement object) causes a change in the total capacity. If an AC current of constant frequency and constant amplitude flows through the sensor capacitor, the amplitude of the AC voltage on the sensor is proportional to the distance to the target (ground electrode). The controller detects through different outputs, processes the change in the distance between the measuring object and the controller, and outputs it as a measured value.

The sensor's structure is shown in Figure 2.3.

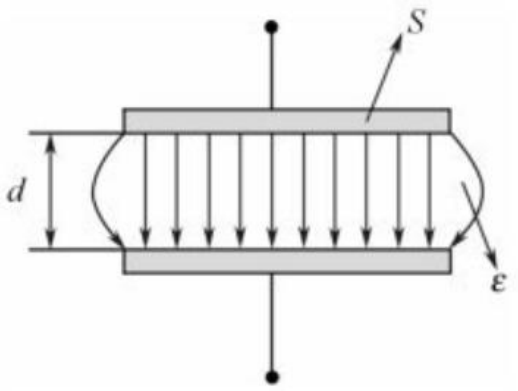

Figure 2.3 capacitive displacement sensor structure. [9]

ε is the dielectric constant of the dielectric between the two parallel plates of the sensor, d is the distance between the upper and lower plates, and S is the relative effective surface area between the upper and lower plates. Ignoring the edge effect between the two plates, the capacitance value between the two plates can be expressed by Equation 2.1.2.1[10]:

$$C = \frac{\varepsilon_r \varepsilon_0 S}{d} \qquad (2.1.2.1)$$

For my opinion: capacitive sensor has good measuring range, resolution, suitable size and operating temperature as well. For example, capacitive sensor CSH2-CAm1,4, it has 2mm measuring range, 1.5nm resolution and maximum 20mm diameter and 200°C operating temperature. Link for the sensor: https://www.micro-epsilon.com/download/products/cat--capaNCDT--en.pdf. However, for most of capacitive sensors 200°C is the maximum temperature they can accept. But there is

still sensor that can meet the high temperature of 250℃, capacitive sensor can be used in this experiment.

2.4 Laser triangulation displacement sensor

The laser displacement sensor is a precision optical instrument based on the principle of laser triangulation measurement.

2.4.1 Working principle of triangulation displacement sensor

The laser emits laser light to the plane to be measured. At this time, the axis of the laser, the optical axis of the imaging lens is located perpendicular to the plane of the photodetector. The receiving lens receives the reflected light and scattered light from the surface of the object, and finally forms an image on the photoelectric position detector. When the surface of the measured object is displaced, the image formed by the photodetector is also displaced correspondingly. Through the relationship between the displacement of the object and its image, the displacement of the object can be calculated. In order to be able to measure accurately, ϕ and θ must meet the Scheimpflug condition [11]. The Scheimpflug principle is a description of the geometric relationship between the orientation of the plane of focus, the lens plane, and the image plane of an optical system (such as a camera) when the lens plane is not parallel to the image plane. According to the angle of the incident laser beam relative to the measured plane, laser triangulation can be divided into vertical triangulation and oblique triangulation, as shown in Figure 2.4 and 2.5.

Vertical triangulation

The light emitted by the laser is focused by the convergent lens and then incident vertically on the surface of the measured object. The movement of the object or the surface change causes the incident light spot to move along the incident optical axis. The receiving lens receives the scattered light from the incident light spot and images it at the position of the light spot detector.

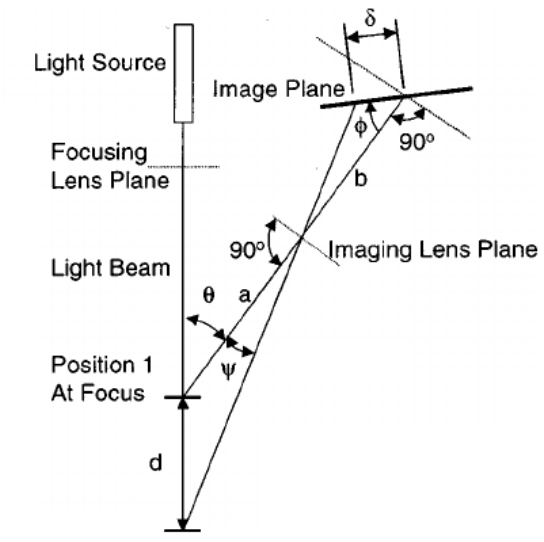

Figure 2.4 vertical triangulation principle [12].

Oblique triangulation

The light emitted by the laser is incident on the measured surface at a certain angle with the normal direction of the measured surface, and the scattered light or reflected light of the light spot on the measured surface is also received by the receiving lens.

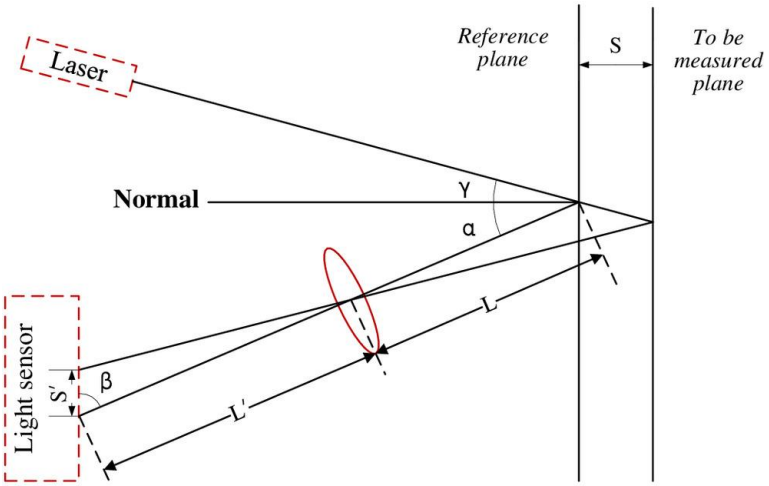

Figure 2.5 oblique triangulation principle [13].

From the above principal analysis, it can be seen that the two laser incident measurement methods meet the requirements for non-contact measurement of the measured target while also ensuring the timeliness, speed, and accuracy of the measurement results. But they still have different advantages and disadvantages in application effects, mainly in the following aspects: (1) If the surface of the object to be measured mainly produces reflected light, since the reflected light is mainly received by the photoelectric detector of the oblique system, then the oblique system with good detection capability for objects with high surface reflectance should be the first choice. For the vertical triangulation system, since it can only receive the light scattered from the surface of the target to be measured, the measurement target with better scattering is more suitable for the direct system. (2) Comparing Figure 2.4 and Figure 2.5, it can be seen that when the measured object is displaced in the oblique type, the light spot illuminates different positions on the surface of the object, so the displacement of the measured object cannot be calculated directly based on the image shift, while the position of the direct light spot is Fixed, can be measured directly.

For my opinion: triangulation sensor has good measuring range, resolution and suitable size. For example, triangulation sensor ILD1750-2. It has 2mm measuring range, 0. 1μm repeatability, < ±1.6μm linearity and 45x31mm in size. Link for the sensor: https://www.micro-epsilon.com/download/products/cat--optoNCDT--en.pdf. However, all triangulation sensors do not have good heat resistance. The highest temperature it can withstand is only 70°C, even with the protection of heat-resistant materials, it cannot meet the experimental requirements. Triangulation sensor cannot

be used in this experiment.

2.5 Interferometers

2.5.1 Monochromatic light interference characteristics

When the frequency and vibration direction of the two rows of light waves are the same, the phase is the same or the phase difference is constant, if superposition occurs, the vibration of some points will always be strengthened, and the vibration of other points will always be weakened, resulting in stable streaks of alternating light. The phenomenon is the interference of light. When two rows of light waves satisfying the interference conditions (light source positions P1, P2) interfere at a certain point O, they will enhance each other after interference, and the intensity of the combined beam will increase, shown in Figure 2.6.

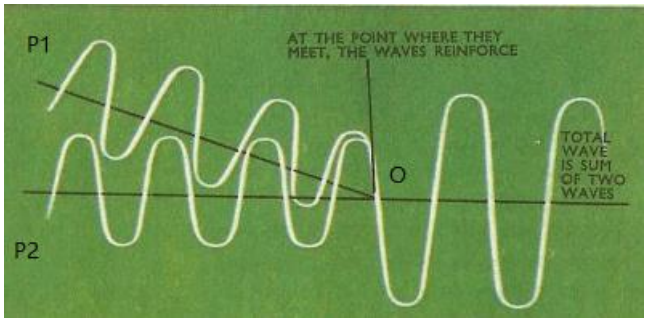

Figure 2.6 Two beams of light interfere [14].

their resonance equations can be obtained from Wave Optics as follows [15]:

$$y_1 = a_1 \cos(\omega t + \varphi_1) \tag{2.5.1}$$

$$y_2 = a_2 \cos(\omega t + \varphi_2) \tag{2.5.2}$$

The distances from point O to P1 P2, are L1 L2, respectively. If the amplitude attenuation in the propagation process is neglected, the vibrations from P1 P2 to point O are:

$$y_{o1} = a_1 \cos(\omega t + \varphi_1 - 2\Pi L_1/\lambda) \tag{2.5.3}$$

$$y_{o2} = a_2 \cos(\omega t + \varphi_2 - 2\Pi L_2/\lambda) \tag{2.5.4}$$

Where λ is the wavelength of the light wave

Then by formulas (2.4.3) and (2.4.4), the resultant vibration of point O can be obtained as:

$$y_0 = a_1 \cos\left(\omega t + \varphi_1 - \frac{2\Pi L_1}{\lambda}\right) + a_2 \cos\left(\omega t + \varphi_2 - \frac{2\Pi L_2}{\lambda}\right) = A\cos(\omega t + \theta) \tag{2.5.5}$$

The square of the combined amplitude is:

$$\begin{aligned} A^2 &= a_1^2 + a_2^2 + 2a_1a_2[\cos(\varphi_1 - \varphi_2) - 2\Pi(L_1 - L_2)/\lambda] \\ &= a_1^2 + a_2^2 + 2a_1a_2(\cos\varphi - 2\Pi\Delta/\lambda) \\ &= a_1^2 + a_2^2 + 2a_1a_2\cos\delta \end{aligned} \tag{2.5.6}$$

Where the initial phase difference: $\varphi = \varphi_1 - \varphi_2$, optical path difference: $\Delta = L_1 - L_2$ (medium is air and refractive index=1), phase angle: $\delta = \varphi - 2\Pi\Delta/\lambda$.

Since the light intensity is inversely proportional to the square of the amplitude, the combined light intensity is:

$$I = I_1 + I_2 + 2\sqrt{I_1 I_2}(\cos\varphi - 2\Pi\Delta/\lambda) \quad (2.5.7)$$

Generally, the two columns of light waves in an interferometer are emitted by the same light source, therefore, $\varphi = 0$, then the interference light intensity distribution law of the general interferometer is:

$$I = I_1 + I_2 + 2\sqrt{I_1 I_2}(2\Pi\Delta/\lambda) \quad (2.5.8)$$

2.5.2 White light interference characteristics

The white light source contains continuous spectral components in the entire visible spectrum, and its wavelength range is 400-700nm. As shown in Figure 2.5.1, when white light interferes, light waves of each wavelength will generate a set of interference fringes, and the light intensity distribution law conforms to the formula (2.5.8). Since the spacing of the interference fringes is dependent on the wavelength of the light waves, the zero-level fringes of each wavelength will only coincide when the optical range difference Δ = 0. Here the zero-level stripe with the highest contrast is formed, which is the best position for interference. The interference fringes of the wavelengths are gradually staggered as the optical range difference increases, and the contrast decreases until it disappears completely. The wider the wavelength range of the light source, the more pronounced this decrease in contrast becomes.

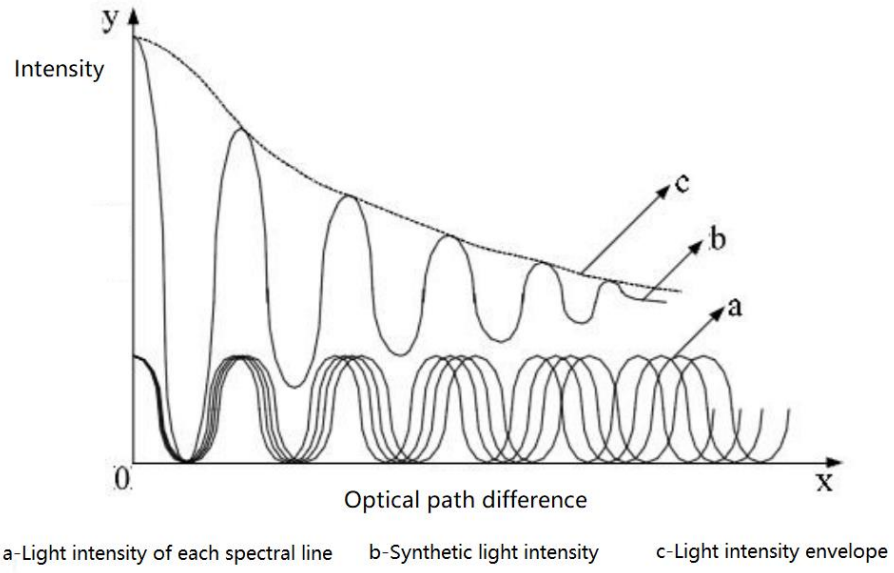

Fig. 2.6 Resultant curve of white light interference fringe intensity [16].

The measured light intensity I in white-light interferometry is a function of the reference mirror scanning position z and the height of the sample's reflectance layer z_0 [17].

$$I(z) = \int_{\lambda_2}^{\lambda_2} A(z - z_0)\, B_{Led}(\lambda) B_{Cam}(\lambda) e^{j(k(z-z_0)+\Phi)} d\lambda \quad (2.5.9)$$

$$(k = 2\Pi/\lambda)$$

where, λ is the wavelength over which the intensity of the light is integrated,

$B_{Led}(\lambda)$ is the complex bandpass of the LED light source,
$B_{Cam}(\lambda)$ is the complex bandpass response of the camera,
A is the statistical reflection function, which is affected by surface roughness.

2.5.3 Principle of white light interferometry

White light interferometry is a technique that takes advantage of white light interference's typical features. The position of the measured surface or the reference mirror is changed by scanning in order to locate the position of the zero-light-range near point on the measured surface, and the discrete data curve of the change of the light intensity (grey value) at that point is obtained. In white light interferometry, the difference in the optical range of the corresponding two columns of light waves is zero if the distance from the beam splitter to a point on the measured surface is equal to the distance from the beam splitter to the reference surface. The interferometric light intensity value reaches its maximum at this point. The light intensity value at each position varies as the PZT (Piezoelectric transducer) moves the table one step throughout the measurement. A CCD camera is used to collect photos of the interference stripes, which are then saved in a computer. The interferogram data is then analyzed using a zero-light-range nearness recognition algorithm to extract the peak of the coherence envelope at each pixel point, i.e. the zero-light-range nearness, which represents the pixel point's relative height. The overall shape of the surface of the sample under test is then formed by combining the relative heights of all the pixel points, which is then reconstructed in 3D to acquire the surface shape and complete the device surface measurement, See Figure 2-6.

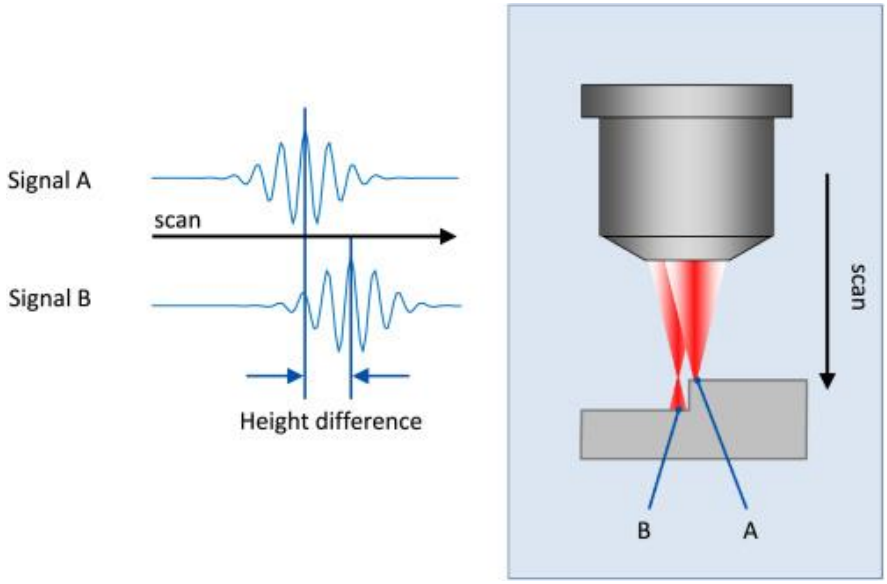

Figure 2.6 Schematic diagram of white-light interference measurement.

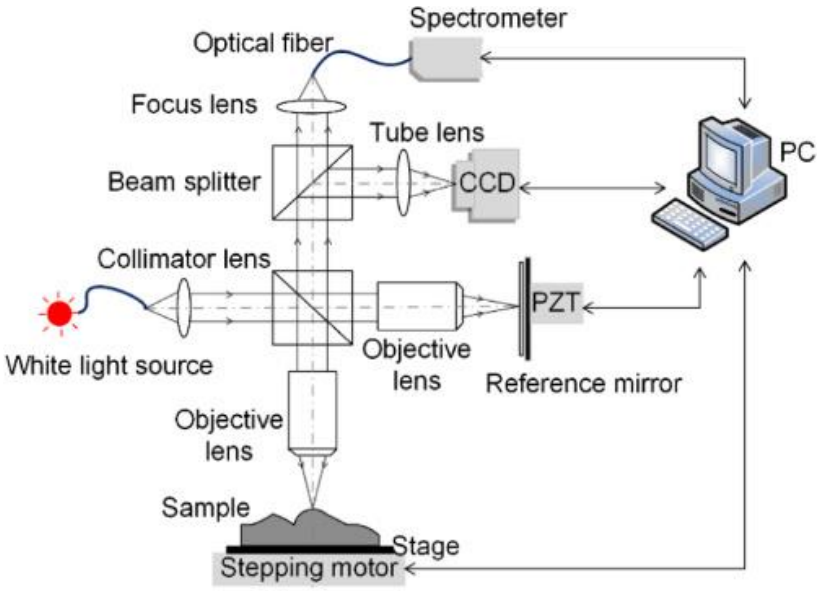

Figure 2.7 Principle of white light interferometer [17][18].

For my opinion: for example, interferometers IMS5600-DS. It has 2.1mm measuring range, < 30pm resolution and 10mm diameter. Link for the sensor: https://www.micro-epsilon.com/download/products/cat--interferoMETER--en.pdf. However, interferometers do not have good heat resistance as well. The highest temperature it can withstand is only 70℃ which is far from the excepted 250℃. Interferometers cannot be used in this experiment.

2.6 Time-of-Flight Sensors

TOF (Time of Flight) is a method of distance detection through the flight time of light.

2.6.1 Principle of TOF Sensors

The basic principle of TOF is that a modulated light pulse is emitted by an infrared transmitter. When the light pulse encounters an object and is reflected, the reflected light pulse is received by a receiver. The distance to the object is calculated from the round trip time of the light pulse. In practice, this is usually modulated as a pulse (or sine wave). When an obstacle is encountered and diffuse reflection occurs, the reflected pulse (or sine wave) is picked up by a special CMOS sensor. By this time the waveform has been offset and the distance from the object to the depth camera can be calculated by measuring the waveform offset [19].

Depending on the method of measurement of the reflected waveform offset by the TOF sensor, there are indirect (phase) and direct (pulse) methods of measurement.

2.6.2 Indirect time-of-flight ranging method

Indirect time-of-flight (I-TOF) does not directly measure the round-trip time of

photons but uses time-gated measurement of light intensity to indirectly infer the round-trip time. Indirect time-of-flight (I-TOF) does not require an accurate time stopwatch. It only needs a time-gated photon counter or a charge integrator. It uses two modulated light source signals to indirectly measure the phase difference, and then calculate the optical flight time. This technology facilitates pixel-level integration on a silicon-based material with a smaller area [20].

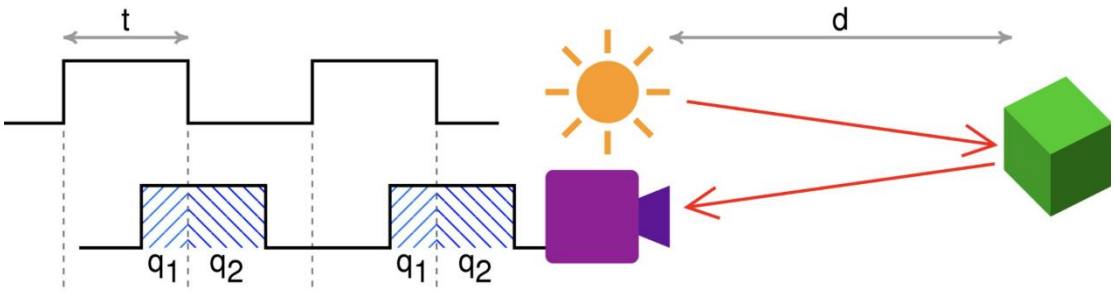

Figure 2.6.1 Schematic diagram of indirect TOF principle [21].

Indirect time-of-flight ranging sensors usually have two accumulation areas in each pixel to demodulate the signal. When the modulating signal is a pulse or an on/off signal, two pulses with delay time [t] are emitted with a repetition frequency [MHz]. For forming many integration parts for the reflected laser pulse, several integration windows need to be defined. Each integration window can achieve detection at different distance ranges after delay.

Figure 2.6.1 illustrates the working principle of indirect time-of-flight (I-TOF). In this method, the TOF signal obtained is as follow figure 2.6.2.

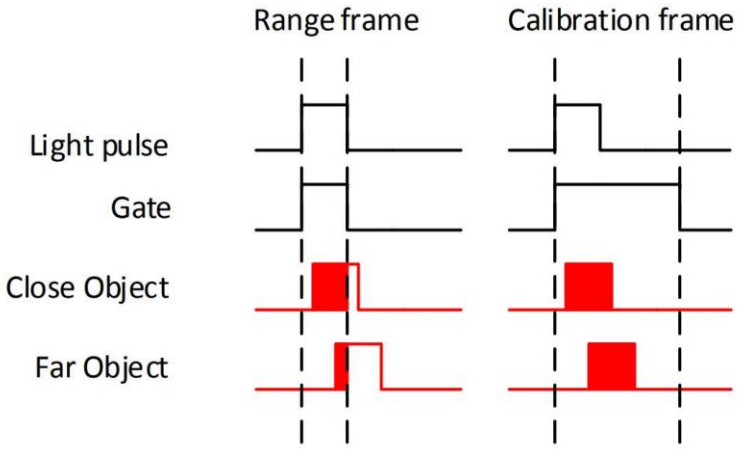

Figure 2.6.2 working principle of indirect time -of-flight [22]

The time it takes for light to travel to the object and back causes the phase shift between the illumination and shutter modulation waveforms. This phase shift is used as part of the entire period, multiplied by the modulation period to give the effective time for the signal to reflect from the object.

$$t = T_{mod}\frac{\Phi}{2\Pi} = \frac{\Phi}{2\Pi f_{mod}} \tag{2.6.1}$$

Φ is due to the phase difference introduced by the light returning after hitting the Object, f_{mod} is the modulation frequency. According to the imaging principle of TOF:

$$d = \frac{vt}{2} \tag{2.6.2}$$

Combined with formula 2.6.1 and 2.6.2, the final indirect TOF distance calculation formula is:

$$d = \frac{c\Phi}{4\Pi f_{mod}} \tag{2.6.3}$$

2.6.3 Direct time-of-flight ranging method

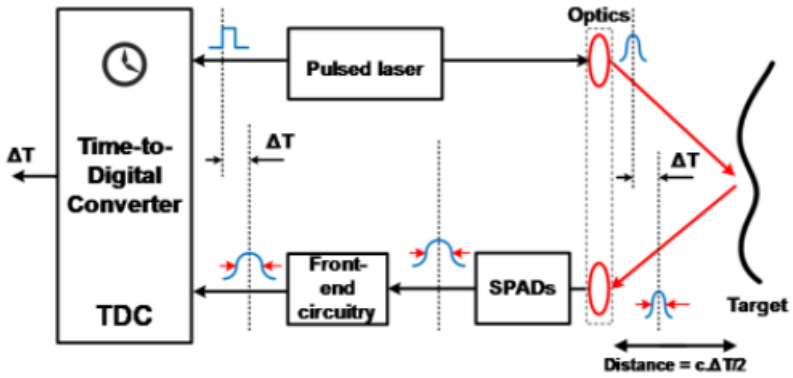

Figure 2.6.3 schematic of direct time-of-flight. [23]

In a direct time-of-flight sensor (D-TOF) shown in figure 2.6.3, the sensor circuit directly measures the round-trip time of the optical signal. The system emits the laser pulse emission signal through the synchronous laser, and the high-precision timer starts timing synchronously. After the light signal is reflected by the sensor's photosensitive pixel, the high-precision timer stops timing, and then directly records the time it takes for the light signal to go back and forth τ_{TOF}. The target distance L can be estimated by the following formula:

$$L = \frac{c}{2}\tau_{TOF} \tag{2.6.4}$$

For my opinion: laser distance sensors for extra-long ranges (TOF) sensor cannot be used in this experiment. For example, TOF ILR1030-8/LC1. It has minimum 0.2m measuring range which is quite large for our case. 1mm resolution is also too low to observe a clear light path. 70℃ operating temperatures will cause the sensor to lose its normal performance when entering the furnace with a temperature of 250℃. Size of the sensor is 54.6x25.8mm which is the only one condition can meet the requirements of the experimental. Link for the sensor: https://www.micro-epsilon.com/download/products/cat--capaNCDT--en.pdf.

2.7 Inductive displacement sensor

Inductive displacement sensor is a newly developed sensor after capacitive

displacement sensor.

2.7.1 The theoretical basis of inductive sensors

The inductive displacement sensor is a sensor that uses the principle of electromagnetic induction to convert changes in mechanical quantities such as displacement and liquid level vibration into changes in electrical quantities through changes in the self-inductance or mutual inductance of the coils, thereby realizing displacement measurement. There are many types of it, which can be divided into self-inductance and mutual inductance (LVDT) according to different conversion principles.

The self-inductive displacement sensor has a relatively simple structure, and it uses the principle that the self-inductance of the coil changes with the measured change. Generally, self-inductive displacement sensors are called inductive displacement sensors. The mutual inductance type uses the mutual inductance coefficient between the primary and secondary coils to change with the measurement. Because it is often made into a differential type and uses the principle of a transformer, it is often called a differential transformer (LVDT).

2.7.2 Self-sensing sensor

The basic structure of a self-sensing sensor is shown in the figure 2.7.1:

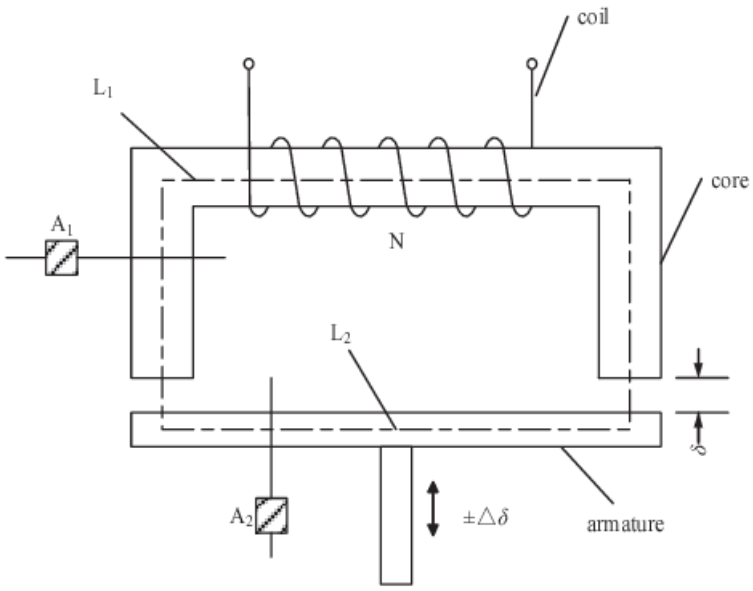

Figure 2.7.1 Schematic diagram of self-sensing sensor [24].

According to the definition of coil inductance

$$L = \frac{\psi}{I} = \frac{N\Phi}{I} \tag{2.7.1}$$

Magnetic flux is defined as

$$\Phi = \frac{NI}{\sum_{i=1}^{n} R_{mi}} \tag{2.7.2}$$

Magnetoresistance

$$R_{mi} = \frac{l_i}{\mu_i A_i} \tag{2.7.3}$$

Combine equations (2.7.1) (2.7.2) and (2.7.3) we can get:

$$L = \frac{N^2}{\sum_{i=1}^{n} R_{mi}} = \frac{N^2}{\sum_{i=1}^{n} \frac{l_i}{\mu_i A_i}} = f(l_i, \mu_{i,} A_i) | N = constant \tag{2.7.4}$$

L - inductance of the coil; N - number of turns of the coil.
A_i - cross-sectional area of each section of the magnetic conductor.
Φ - magnetic flux.
I - current in the coil.
R_{mi} - reluctance of the i-th section of the magnetic circuit.
μ_i - coefficient of permeability of the i-th section of the magnetic circuit.
l_i - length of the i-th section of the magnetic circuit.
n - number of sections of the magnetic circuit.

The above equation shows that the coil inductance is a function of the three variables μ, a and i when the number of turns of the coil is certain. If two of these variables are fixed, the inductance is a single-valued function of the other variable and constitutes a form of sensor. Inductive sensors are therefore available in three operating modes: variable gap, variable area and solenoid.

Their working principle: the change in magnetoresistance, the change in relative coverage area, the change in the length of the reach in the coil in the sensor, resulting in a change in inductance in the coil, thus determining the direction and size of the displacement of the object being measured [25].

2.7.3 Mutual inductance sensor

The principle of the mutual inductance sensor is to convert the measured displacement into the change of mutual inductance between coils. The sensor itself is equivalent to a transformer. When the primary coil is connected to the power supply, the secondary coil generates induced electromotive force. When the mutual inductance changes, the induced electromotive force also changes accordingly. Since the sensor is often made into a differential form, it is called a differential transformer type sensor.

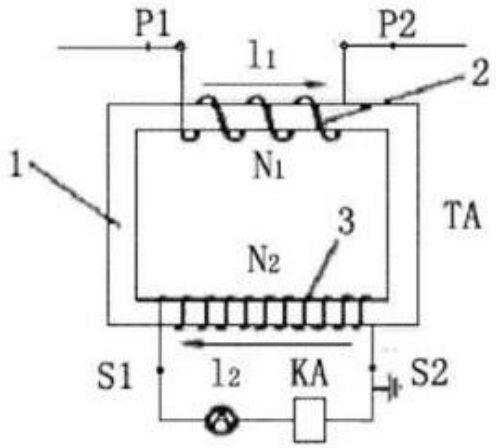

Fig. 2.7.2 Structure of the mutual inductive sensor [26].

For my opinion: inductive sensor has good measuring range, resolution and suitable size. For example, inductive sensor DTA-1G8. It has ±1mm measuring range, ≤0.15 repeatability, ≤ ±6μm linearity and 8mm diameter. Link for the sensor: https://www.micro-epsilon.com/download/products/cat--induSENSOR--en.pdf. However, inductive sensors do not have good heat resistance. The most temperature it can withstand is 80℃. When inductive sensor is protected by suitable heat-resistant materials, its operating temperature can be 200℃, but it cannot get higher than 250℃, so it is not suitable for the conditions required for the experiment.

2.8 chromatic confocal sensor

2.8.1 Chromatic confocal measurement principle

The principle of chromatic confocal displacement measurement is derived from the classical confocal microscopy technique, which is based on the confocal microscopy technique with the addition of a new optical method-the color coding technique. The depth of focus is thus extended, solving the problem of the very small depth of focus in confocal microscopy, allowing it to be applied to displacement measurements and retaining the advantages of the high signal-to-noise ratio and high resolution of confocal microscopy.

The structure of a spectral confocal displacement measurement system based on a spectroscopic prism is shown in Figure 2.8.1. The light from the white light source W passes through the pinhole P and can be approximated as a point light source. Light from the point source passes through a splitter prism B and a dispersive objective L. Since the optical properties of the dispersive objective are wavelength dependent, a series of continuously distributed focused spots of different wavelengths are formed on the optical axis, which is also known as color coding [27].

When the sample under test is placed at point M within this color-coded segment, the surface of the sample under test contains all the spectral information. Since the surface of the sample under test scatters the incident beam, the scattered light passes

again in the opposite direction through the dispersive objective and the spectroscopic prism and reaches the spectrometer. The pinhole P' plays a vital role in the structure, and it is used to prevent the entry of all beams except the M point, especially the light points higher or lower than the M point on the optical axis. It is precisely because of this principle of point detector focusing and imaging that the spectral confocal displacement sensor has excellent spatial resolution and is not sensitive to surrounding stray light. Since the location of the pinhole P' and the location of the pinhole P are conjugated to each other, the point M is its confocal point. When the sample under test moves up and down within the focal spot range of different wavelengths, a confocal system of different wavelengths is formed at each position.

Since the wavelength spot size that satisfies the confocal condition is small and the energy distribution is relatively concentrated, the light flux passing through the pinhole is large. While other wavelengths are in a defocused state, the spot size is large, and the energy distribution is relatively dispersed, so the light flux passing through the pinhole is small. Through the multi-channel detection function of the spectrometer, it can realize the distributed measurement of multiple probes. Combined with the corresponding software algorithm, the signal obtained from the spectrometer is analyzed and processed, so as to know the wavelength value at the maximum luminous flux, and then obtain the position of the measured object.

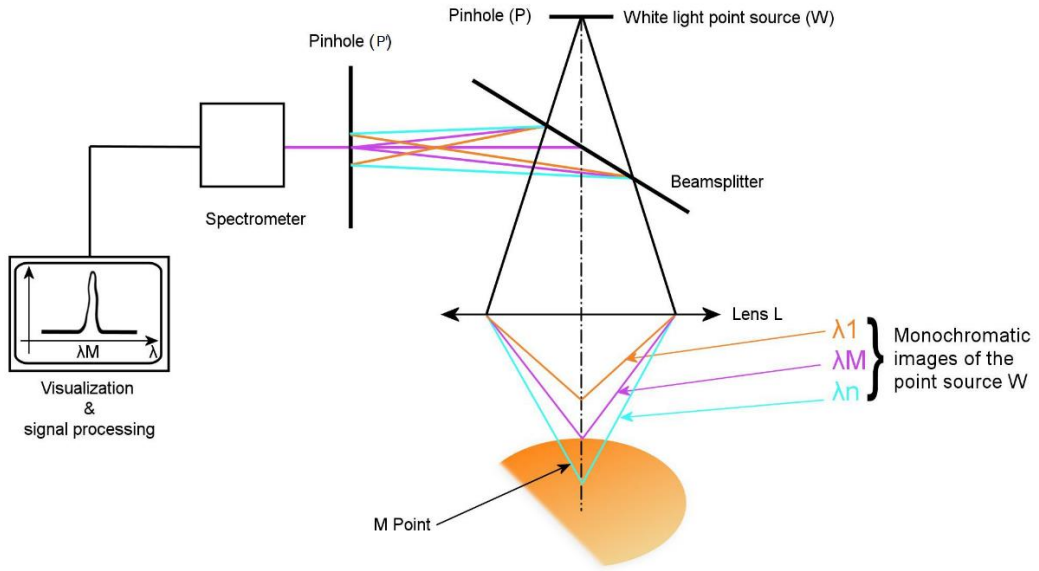

Figure 2.8.1 Structure of spectroscopic prismatic chromatic confocal displacement measurement system [28].

In order to achieve the miniaturization of the system, a fiber coupler is usually used instead of pinholes to filter light, as shown in Figure 2.8.2. Optical fiber has the advantages of wide transmission frequency, low loss, small size, light weight, strong anti-electromagnetic interference ability, high fidelity, reliable working performance, and fast transmission speed. Through the optical fiber optical path structure, large light sources, spectrometers and other equipment can be placed far away from the probe, which can greatly reduce the size of the probe.

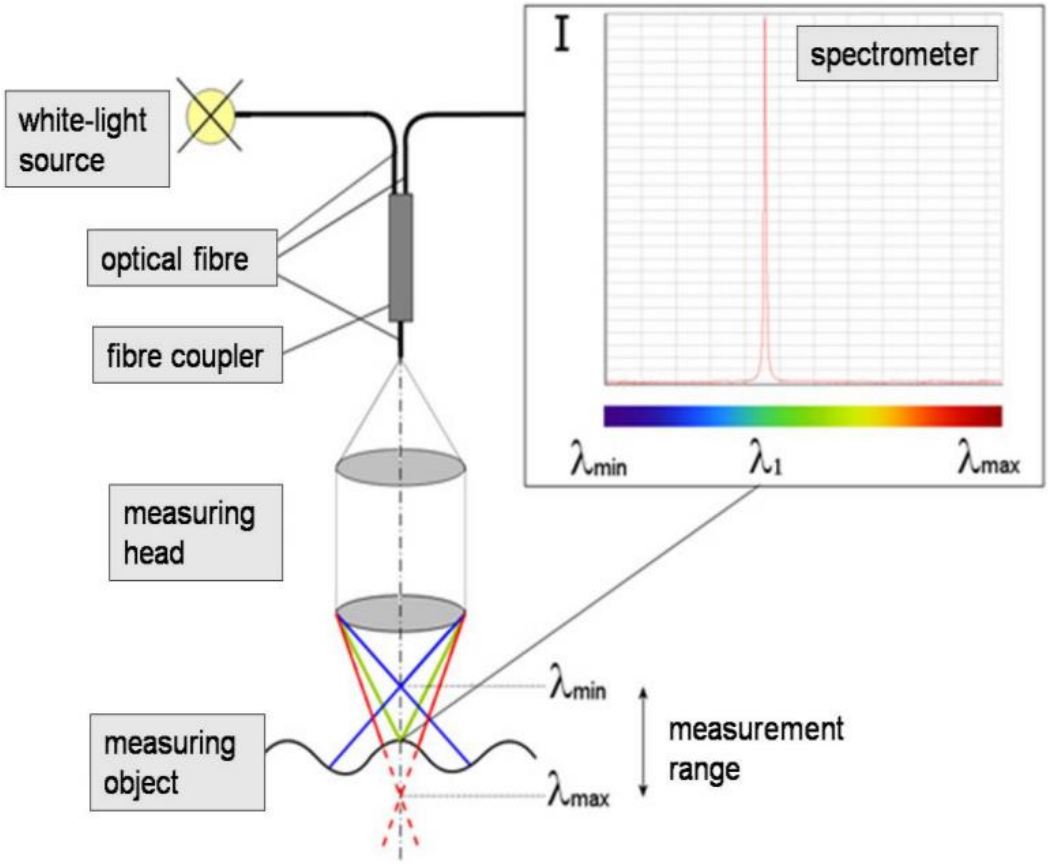

Figure 2.8.2 Structure of optical fiber coupler type chromatic confocal displacement measurement system [29].

For my opinion: chromatic confocal sensor has good measuring range, resolution, suitable size and operating temperature. For example, chromatic confocal sensor confocalDT IFS2404 IFS2404-2. It has 2mm measuring range, 40nm resolution and 12mm diameter. Although its operating temperature is 70℃ in terms of parameters, it can increase the thermal resistance to 250℃ by adding heat-resistant materials. Link for the sensor: https://www.micro-epsilon.com/download/products/cat--confocalDT--en.pdf. Chromatic confocal sensor can be used in this experiment.

3 Fiber optic displacement sensor

Fiber optic displacement sensors are multifunction devices that have applications in a variety of industries, including automotive, aerospace, military, and medicine. Optical-fiber-based displacement sensors are appealing because of their ability to function in hostile settings, such as cryogenic to higher temperatures, under vacuum, or in the presence of severe vibrations. For these reasons, these instruments are widely employed in aeronautics and aerospace, nuclear power plants, robotic systems, civil engineering and geotechnical measurements, and a variety of other hazardous or hazardous site applications [30].

In general, such sensors are most often employed to measure and/or monitor

relative movement (displacement). They can, however, be used as sensors for position, thickness, concentricity, alignment, proximity, rotation, and torque, among other things. They can also make measurements by direct contact or non-contact, depending on their design and configuration.

Fiber optic displacement sensors are routinely designed using a variety of ways. The following are a few of the most common:

- Reflective technology
- Microbending technology
- Modulating technology
- Fabry-Perot technology
- Fiber Bragg grating technology

The optical fiber displacement sensor is a device that uses the displacement to modulate the light wave parameters delivered in the optical fiber, then demodulates and detects the modulated light wave signal to obtain the measured displacement value. Figure 3.1 depicts its structure, which is made up of five parts: a light source, an optical fiber, an optical sensor head, photoelectric conversion, and a signal processor. The optical sensing element is impacted by the surrounding displacement field to modify the light transmitted in the optical fiber, and the light emitted by the light source enters the optical sensing element through the optical fiber. The photoelectric conversion of the light wave holding the information to be measured is then delivered to the signal processor for processing, which then restores the change in the measured displacement.

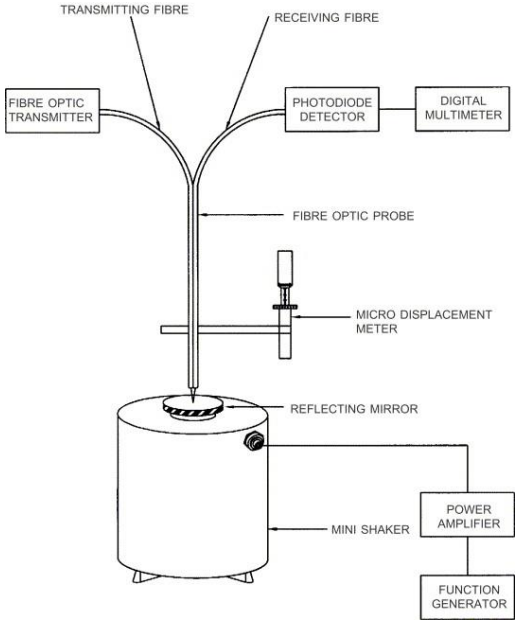

Figure 3.1 structure of fiber optic displacement sensor [31].

3.1 Reflective fiber optic displacement sensor

Optical fiber is an important application of total reflection phenomenon. The optical signal is transmitted to the reflecting surface through the optical fiber of the light source. It will form a communication in the three-dimensional space to recognize the reflected light cone. Only when the receiving optical fiber collects the reflected light

signal within its coverage; otherwise, no signal is collected. Figure 3.2 depicts the basic principle of a reflecting sensor. Two fiber optic legs make up the sensor (bundles or single fiber). One leg transmits light to a reflecting target, while the other leg captures and transmits reflected light to a detector.

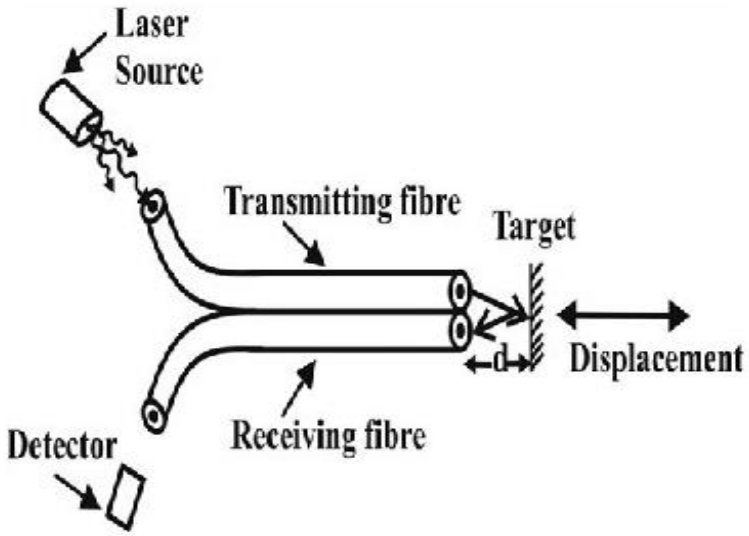

Figure 3.2 Reflective fiber optic sensor [32].

The intensity of the measured light is proportional to the distance between the reflecting target and the fiber optic probe. Figure 3.3 displays the fundamental response curve. The curve has a high linear front slope and a $1/R^2$ rear slope, where R is the distance between the fiber optic probe tip and the reflecting surface.

When considering geometric optics, the curve is simple to comprehend [33]: light exits the transmitting fibers in a solid cone defined by the numerical aperture. The size of the target-hitting spot is regulated by (assuming the fiber is small in relation to R)

$$D = 2Rtan\theta \tag{3.1}$$

Where D is the spot diameter and 0 is the half angle between the normal of the fiber exit surface and the exit divergence cone (numerical aperture).

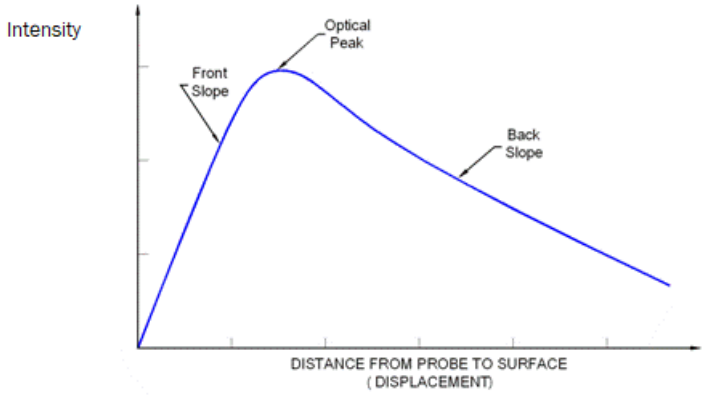

Figure 3.3 Reflective fiber optic sensor response curve [34].

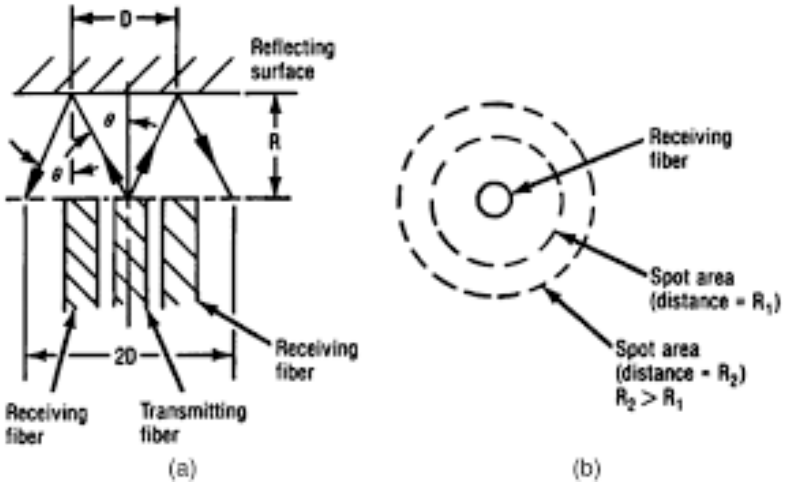

Figure 3.4 Back slope considerations. (a) Fiber target geometry and (b) reflected spot area [35].

The spot size reflected back to the fiber optic probe after reflection is twice the size of the spot that first hit the target, because the angle of reflection is equal to the angle of incidence. The area of the spot expands in a direct proportionate to R as the distance from the reflecting surface increases (see Fig. 3.4). Because the receiving fiber is constant in size and less of the fiber face intersects the returning light as it expands with distance, the amount of detected light is inversely proportional to the spot area or $1/R^2$. As the probe tip approaches the reflecting target, it reaches a point where the reflected light rays are no longer connected with a receiving fiber. As seen in Fig. 3.5, a maximum forms at the commencement of this occurrence (position 2), which then declines to zero as the reflecting surface hits the probe.

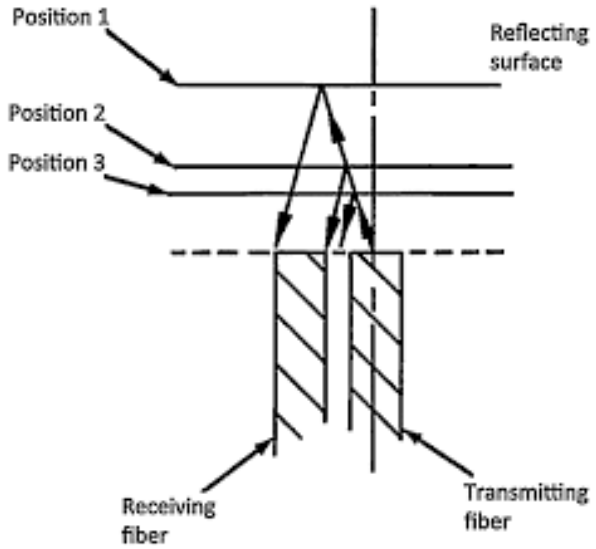

Figure 3.5 Front slope considerations [35].

3.2 Microbending Technology

The optical fiber microbend sensor is based on the optical intensity loss caused by the axial bending of the optical fiber and the mechanism of the optical fiber

macrobending loss is similar, and it also originates from the spatial filtering and mode coupling effects. When the fiber is bent, mode uncovering occurs, and guided mode scattering is a radiation mode, but the dominant role is not spatial filtering but mode uncovering, that is, the guided mode transmitted in the core radiates out of the fiber [36].

The optical fiber micro-bending sensor is a kind of optical fiber sensor with intensity modulation function. Figure 3.6 is the principle diagram of the optical fiber micro-bending loss intensity modulation.

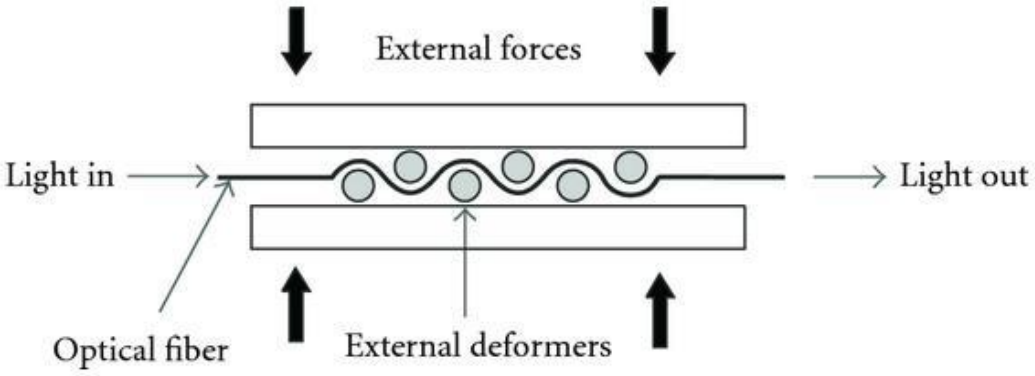

Figure 3.6 Schematic diagram of optical fiber microbend sensor [37]

The optical fiber micro-bend sensor is very sensitive to the small displacement between the toothed plates. At the same time, the dynamic test range of the sensor is also very large, which is also a major advantage of this type of sensor. Therefore, optical fiber microbend sensors are often used as contact sensors for side testing of small displacements in mechanical systems.

3.3 Fiber Fabry-Perot interferometers

The fiber-optic Fabry-Perot (Fabry-Perot, F-P) sensor is made up of two components: the sensing probe and the sensing demodulation device. The fiber optic Fabry-Perot (F-P) sensor probe is the central component of the fiber optic Fabry-Perot (F-P) sensor system. The fiber optic F-P sensor is classified into two types based on the construction of the F-P sensor head: intrinsic fiber F-P sensor and extrinsic fiber F-P sensor. The cavity of the Inherent Fabry-Perot Interferometer (IFPI) is a sensing fiber that measures and transmits data to external elements by changing the distinctive properties of light in the fiber. It has the properties of unity of transmission and sensing, and information collection and transmission are all done in the optical fiber. The cavity of the non-intrinsic fiber F-P sensor (Extrinsic Fabry-Perot Interferometer, abbreviated as EFPI) is an air gap, and the fiber solely transmits light and does not sense the outside environment to be measured.

The optical fiber F-P sensor is classified into two types based on its demodulation mechanism: intensity demodulation type optical fiber F-P sensor and wavelength demodulation type optical fiber F-P sensor.

3.4 Fiber Bragg Grating displacement sensor

Bragg gratings can be utilized as displacement sensors by measuring the strain caused in the grating along its axial direction, resulting in a wavelength change proportionate to the applied displacement (or position). 1 percent strain is within the proof-test level for a common silica fiber. The strain level equates to 1 cm displacement for a 1-m fiber. The practical limit is around 2% strain, or a displacement limit of 2 cm. Designers have used spring-loaded devices to scale this up to measure displacements on the order of several centimeters while reducing the length of measuring fiber required.

Figure 3.7, for example, depicts a schematic of an FBG-based displacement sensor with a spring-loaded sliding rod. One end of the fiber grating is attached to the body of the sensor, which also serves as the device's anchoring or reference point. The other end of the fiber is attached to a spring by a metal wire, which is attached to a sliding rod, which is finally attached to an external point or the item under measurement. The spring constant adjusts the effective force-and consequently the strain-seen by the FBG element.

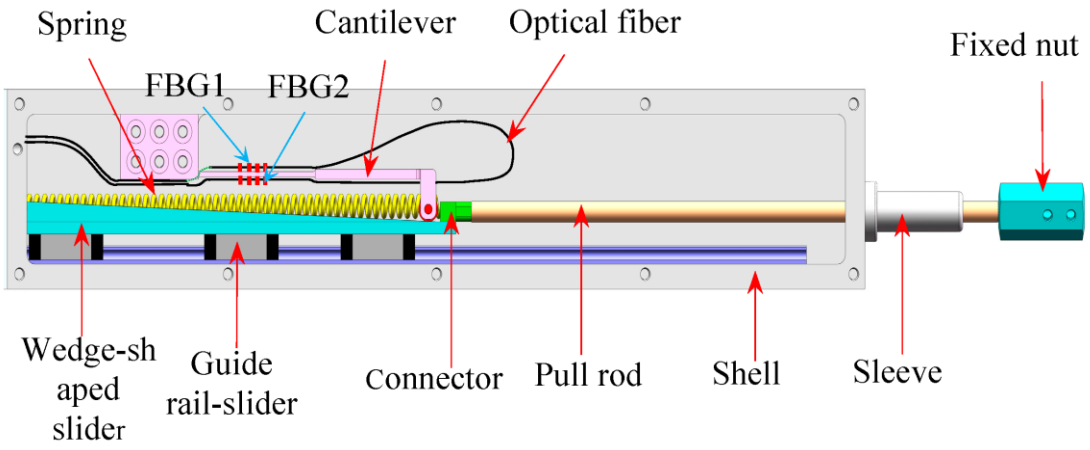

Figure 3.7 A spring-loaded sliding rod is used in the construction of an FBG-based displacement sensor [38].

As the sliding rod advances out, it strains the FBG, causing its peak wavelength to shift spectrally toward longer wavelengths. As demonstrated in Fig. 3.8, the device is extremely linear and reproducible, and it can function in uni- or bi-directional modes. Such displacement sensors typically have a stroke travel of 10 cm and a resolution of 0.05 percent full scale [39]. A second grating is linked in series and insulated from any mechanical strain to compensate for probable temperature effects.

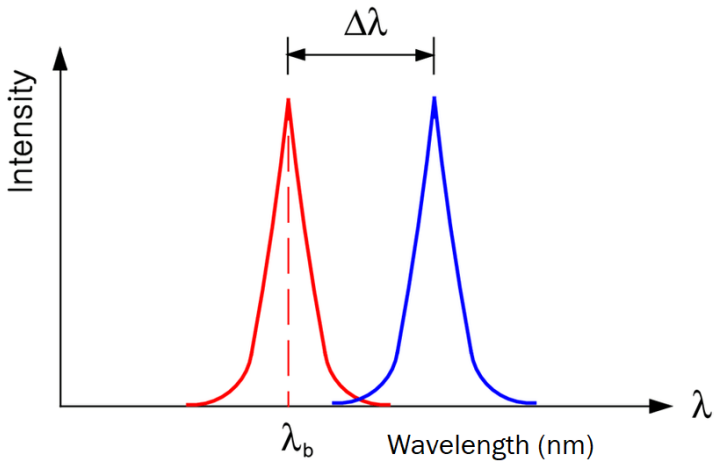

(a)

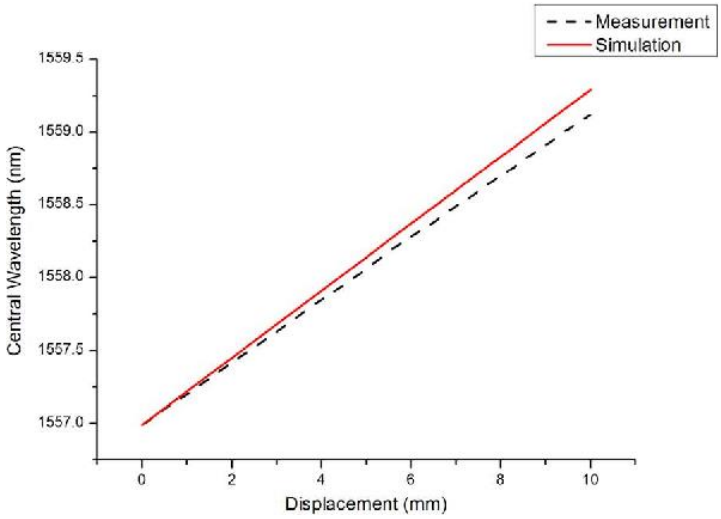

(b)

Figure 3.8 (a) Spectral shift response [40]. (b) Sensitivity curve for the sensor [41]

The strain results in a change in the Bragg wavelength. The magnitude of the shift is proportional to the strain. The system may operate in either a transmissive or reflecting mode, thanks to the employment of a broadband optical source. The return signal can be detected using a coupler, or the transmission spectrum, which also depicts the wavelength change, can be watched.

The Bragg grating responds to strain as well as temperature. Strain causes the fiber to elongate, causing the grating spacing to change. Due to dimensional changes in the radial direction, it also generates a refractive index shift related with Poisson's effect (photoelastic effect). Thermal expansion occurs when the temperature changes, causing the grating spacing to shift.

4 Sensor selection

The sensor required for this experiment needs to meet the following characteristics.

Measuring range: about 2*mm.*

Sensitivity: about 1μm.

Operating temperature: around 250℃ for 2-3 mins.

Diameter of the sensor must be smaller than 80mm.

4.1 Suitable sensor selection

After communicating with the manufacturer and combining the conditions required for the experiment, the following sensors can be used after being enhanced.

1. Confocal Displacement sensor CL series from company KEYENCE. They can be used under 250℃ for about 2-5mins and they have very good resolution. They can all be used in experiments, and their only difference is the measurement range.

   For example:

   CL-L007

   Measuring range in normal mode: ±1.5 mm

   Measuring range in high accuracy mode: ±0.5mm

   Resolution: 0.25μm

   CL-L015

   Measuring range in normal mode: ±1.3 mm

   Measuring range in high accuracy mode: ±0.5mm

   Resolution: 0.25μm

2. Capacitive displacement sensors capaNCDT series CSH2(20)-Cam1.4 from company Micro-Epsilon. This is one updated version that can work at 250℃ but the cable is still only 200℃ resistances. If we know how to cool it this will be a good choice, if we cannot then the manufacturer will make a even better one for us.

   CSH02(20)-Cam1.4

   Measuring range: 0.2 mm

   Resolution: 0.15 nm --- static 2 Hz

   4 nm --- dynamic 8.5 kHz

   operating temperature: 0-250℃

5 Design of chromatic Confocal Displacement Sensor System

In order to achieve the miniaturization of the system, a fiber coupler is used

instead of pinholes to filter light shown in figure 5.1 [50]. The chromatic confocal displacement measurement system mainly includes four parts: white light source, confocal optical system, spectrometer and computer. The confocal optical system consists of a dispersive objective lens and a fiber coupler group.

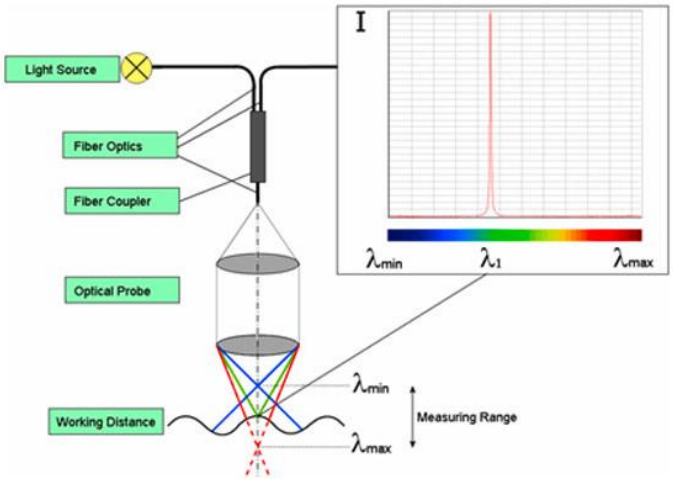

Figure 5.1 The ideal model of chromatic confocal sensor [50].

5.1 Experimental instrument selection and system build

Choose two ready-made lenses to form the system, as shown in Figure 5.1. They will be placed face to face in the designed device.

Figure 5.2 Two lenses used for the system.

The reason why two lenses are used to form a dispersive objective lens is because the sensor can be located at the focal point of the achromatic lens, so that the optical path is formed from the focal point to the parallel light and then to the focal point. The use of double lenses can make all different wavelengths of light can be detected.

The lens on the left is a dispersive focusing lens named with PCX lens (plano-convex). Its flat part faces the object to be measured because what is observed through this direction is clearer and the resolution is high. Why is it high resolution? Put the PCX lens on the collimator platform and observe the images shown by the collimator in the plane direction and aspheric direction of the PCX lens respectively. It is found that the image observed from the plane direction is clearer than the image observed from the aspheric surface Generally, optical systems usually adopt various methods to suppress chromatic aberration and improve image quality. However, for the dispersive objective lens, the material and structure of the components must be reasonably configured to achieve linear dispersion in the axial direction. The lens on the right is a achromatic lens, in our setup used as a collimator. Inside it we can see that it is Carl Zeiss Jena lens. It is Tessarr 2.8/50 (f/number is 2.8, focal length is 50mm) and it's serial number is 8846341. Its focus is on the light source, collimating the white point light source into parallel light. This collimator is removed from an optical instrument. Because it is a manufactured optical instrument, the spherical aberration and chormatic aberration are known, but assumed to be corrected.

5.1.1 Selection of Dispersive Focusing Lens

Because the dispersive focusing lens must be corrected for the prevalent aberration, which is the spherical aberration,we chose an aspheric lens. The radius of curvature of an aspheric lens changes with distance from the optical axis, which is its most distinguishing geometric characteristic. The problem that a spherical surface's optical power varies with a ray height due to the uniform radius of curvature is fundamentally changed. As a result, the spherical aberration can be effectively rectified and the light can be converged to a point.

The aspheric expression is formed by superimposing a series of high-degree polynomials on the basis of conical surfaces such as ellipsoid, hyperboloid, ellipse, and circle. The most commonly used in the design of optical systems is the even-order aspheric surface equation, and its expression is [51]:

$$z = \frac{ch^2}{1+\sqrt{1-Kc^2h^2}} + a_4h^4 + a_6h^6 + \cdots \quad (5\text{-}1)$$

a_4, a_6 ... --- aspheric coefficient
c --- curvature of aspheric vertices
h --- the distance from any point on the aspheric surface to the optical axis
K --- quadric coefficient

By adjusting the surface constant K and aspheric coefficients, the shape of the surface can be controlled to change the direction of the light.

As a result, a single aspheric lens may perform duties that previously required the combination of two or more spherical lenses, and can produce additional effects.

The use of aspheric lenses therefore reduces the number of optical elements required, reduces the size of the system and increases its transmission rate and stability. It also reduces the overall cost of the optical system by eliminating the negative impact on the mechanical parameters that the use of more optical elements might have.

Because the same material has different refractive indexes for different

wavelengths of light, the point light source on the polychromatic axis will focus on different positions on the axis with different wavelengths after passing through the lens. This phenomenon is called axial (or longitudinal) chromatic aberration. Since the function of the dispersive focusing lens is to focus the parallel light to form spectral dispersion, the axial chromatic aberration is the required aberration for the dispersive focusing lens.

Light dispersion leads to undesired chromatic aberration in a lens which expresses in blurring or smearing effect on the objects viewed or "color fringing" around objects viewed. Small Abbe number (higher dispersion) glasses have relatively larger chromatic blur. Lenses that have a higher Abbe number will disperse light less. This produces less chromatic aberration. The Abbe number is defined as [52]:

$$V_D = \frac{n_D - 1}{n_F - n_C} \tag{5-2}$$

The definition refers to refractive indices at three different standard spectral lines in the visible region, which can easily be produced with spectral lamps:
λ_F=486.1 nm (blue Fraunhofer F line from hydrogen),
λ_D=589.2 nm (orange Fraunhofer D line from sodium),
λ_C=656.3 nm (red Fraunhofer C line from hydrogen).
The middle one (from the sodium D line) lies in the region of maximum sensitivity of the human eye. With the Abbe number we can find the Relation to the chromatic dispersion of lenses, one can easily estimate the change of focal length of a simple optical lens made from a material:

$$f_F - f_C = -\frac{f_D}{V_D} \tag{5-3}$$

It shows that the mismatch of focal length values between the blue and red spectral regions is inversely proportional to the Abbe number.

We consider a convex lens on which light is incident on it shown in figure 5.3,

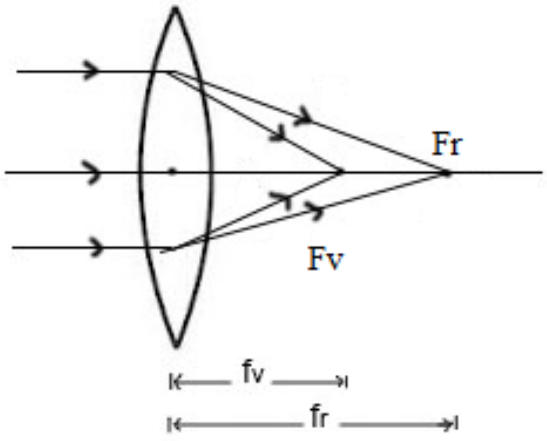

Figure 5.3 white light passes through lens [53].

we know in case of a white light the focal point will be spread between violet and red color focus. And violet focus will be closer and red focus will be farther away, because the refractive index for violet color is more and for red color is less. This separation D

or the spread of the focal point is called longitudinal chromatic aberration for the lens.

$$D=f_r - f_v \quad (5\text{-}4)$$

F_r is foci of red light.
F_v is foci of violet light.
f_r is focal length of red light.
f_v is focal length of violet light.

5.1.2 Filter effect test

We will put various interference filters showen in figure 5.5 close to the front of the PCX, and then measured the corresponding focal lengths. The optical path diagram of the system and the collimator OSK used are shown in Figure 5.4. First we focused the microscope to the last mechanical surface, read its position, the focaused at the focal point, read the position. The back focal length is the different between these two values.

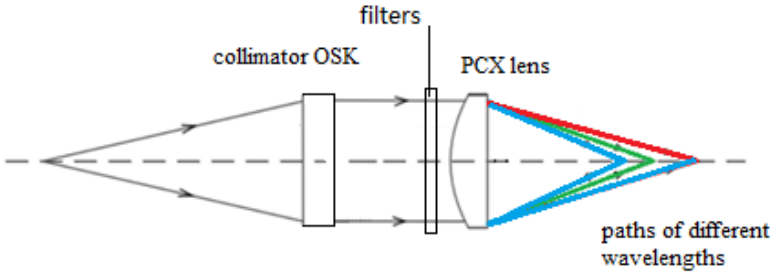

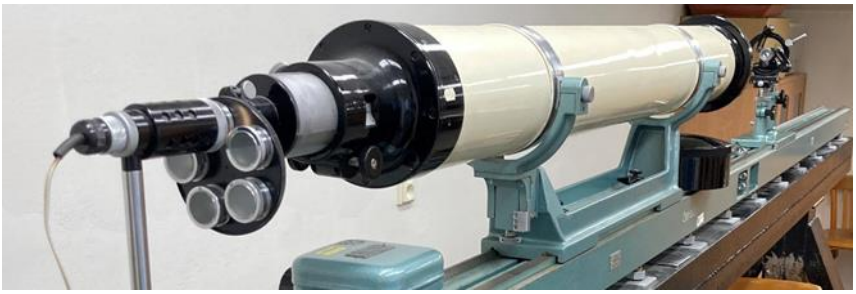

Figure 5.4 Diagram of the Light Path and collimator OSK

Filtter [nm]	Back focal length [mm]
450	13.05
475	13.1
517	13.4
550	13.5
575	13.6
600	13.7
650	13.9
700	14

The relationship between back focal length and wavelength and the longitudinal chromatic aberration is nearly linear,

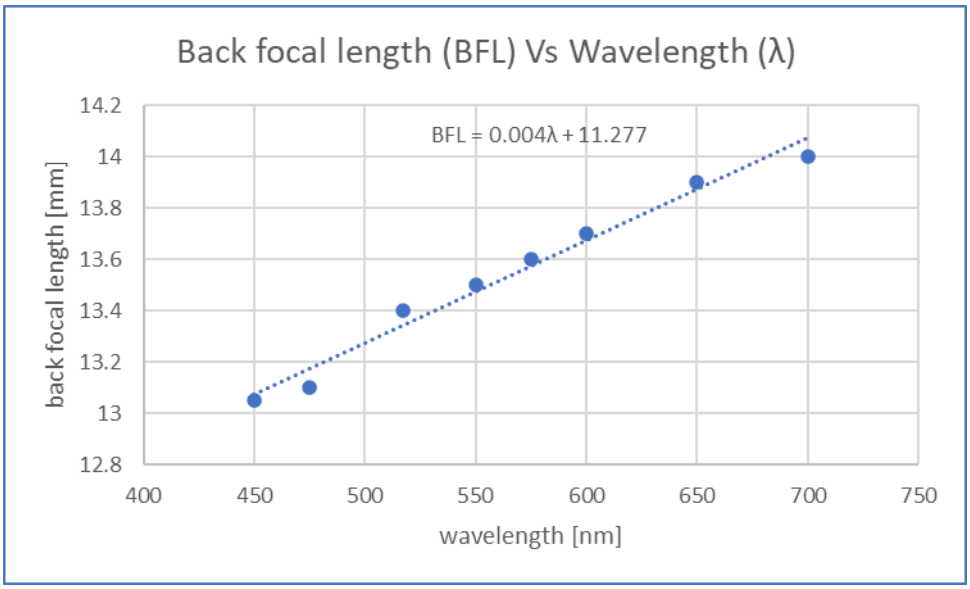

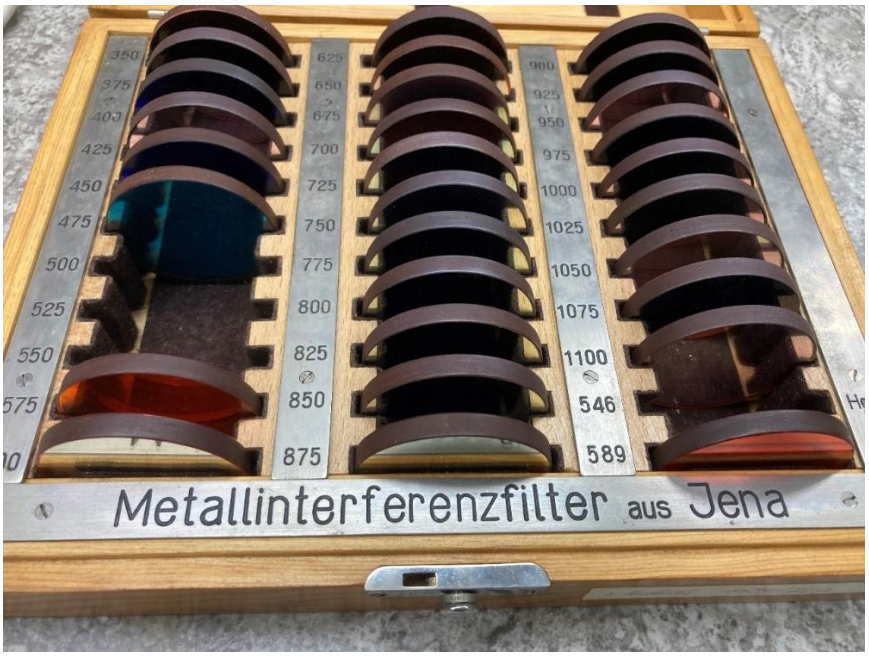

Figure 5.5 filters used in the measurement.

From the measured values we can see the measuring range is around 1mm. Subtract the focal length corresponding to 450nm wavelength from the measured focal length corresponding to 700nm wavelength. From the diagram of relationship between wavelength and back focal length we find when the wavelength changes

from 450nm to 750nm, the corresponding focal length change is 1mm. The sensitivity of the sensor used this lens is not high.

5.1.3 Selection of sensor

Fiber probe used from company Ocean Insight which model is R400-7-SR shown in Figure 5.6. It is a Y type fiber coupler. A fiber optic coupler is a device that can distribute the optical signal from one fiber among two or more fibers or combine the optical signal from two or more fibers into a single fiber. Y coupler is also called tap coupler. This type of coupler simply divides the signal into two outputs. The power distribution ratio between two outputs can be precisely controlled. This Y-type coupler is very suitable for the needs of the experiment. Two input ends are connected to the light source and the other is connected to the spectrometer, and one output end transmits the light into the experimental device and receives the reflected signal to the spectrometer.

Figure 5.6 Fiber probe R400-7-SR [52]

Specifications

	R400-7-SR
Wavelength Range	200nm - 1.1µm
Fiber Core Size	400 µm
Probe Ferrule Diameter	6.35 mm (1/4″)
Numerical Aperture	0.22 ± 0.02 (equivalent to an acceptance angle of 24.8° in air)
Operating Temperature:	-65 to 300 °C

The core diameter of 400µm is thick and it is a multimode fiber. Because of the large core 400µm and also the possibility of large numerical aperture 0.22, this fiber has higher "light-gathering" capacity compared with single-mode fiber and multimode fiber with smaller core diameter. NA (numerical aperature) of the fiber is a very important attribute for the sensor design, it directly determines the minimum diameter of the lens. The relationship between them can be seen from Figure 5.7 [54].

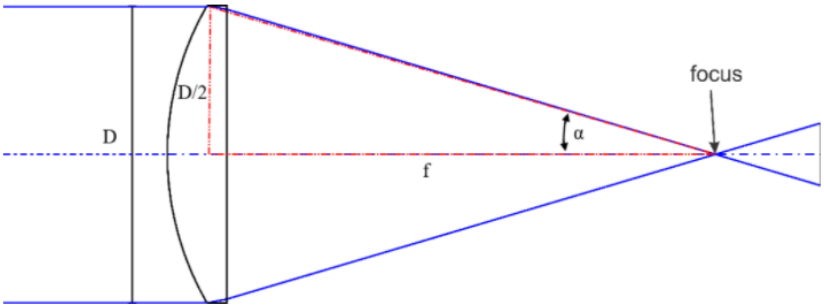

Figure 5.7 simple lens to the right from the focus point there should be the fibre, with the F point exactly at the face of the fibre end.

Numerical Aperture (NA) is the measure of the ability of an optical fiber to collect or confine the incident light ray inside it. It is among the most basic property of optical fiber. Numerical aperture is abbreviated as NA and shows the efficiency with which light is collected inside the fiber in order to get propagated. NA shows the light-gathering ability of the optical fiber and high NA means that the fiber optic "admits" more light.

$$NA=n.sin\theta=\sqrt{n_1^2-n_2^2} \tag{5-5}$$

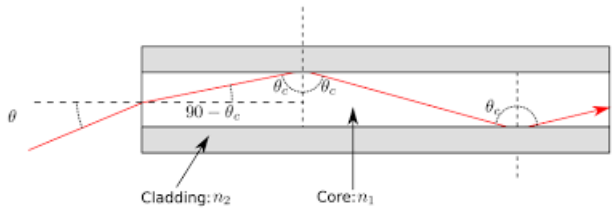

Figure 5.8 A fiber of index n1 with cladding of index n2 [55].

NA is described by the following equation, where n is the medium's index of refraction (typically n=1 for air) and is the half angle of the light cone exiting the lens pupil.

$$NA = n * sin(\alpha) \tag{5-6}$$

In Figure 5.7 we can find simple geometric relationships:

$$\alpha = tan^{-1}(\frac{D}{2f}) \tag{5-7}$$

Now, if we input this definition for into the NA equation, we get:

$$NA = n * \sin(\tan^{-1}(\frac{D}{2f})) \tag{5-8}$$

Put NA= 0.22 into (5-5) can get: α=12.709°

Make (5-8) α=12.709° and f=39.5 mm can get D=17.82 mm. That is much

smaller than the diameter of PCX lens (34 mm). This will cause the sensor to be unable to receive light beyond 17.82mm in diameter. It means we can (and should) stop the lens down to D=18mm. It will decrease residual aberrations and the level of stray light.

5.1.4 Lens properties

We will measure the focal length of PCX lens, determine the locations of its foci using Cornu's method.

Prepare the experimental instrument and fix the PCX lens between the light source and the collimatorr shown in figure 5.9. Apply the powder to the back vertex of the lens, and then focus the microscope on the focal plane of the lens. Focus the microscope on the back surface of the tested lens so that the powder can be seen clearly. The reading difference is x_1. Now apply the powder to the front surface and focus at that. The difference between this point and the back focal point is x_2'. Rotate the lens by 180°, and make the same steps, now rreading x_2 and x_1'. The optical schematics of the experiment is shown in below.

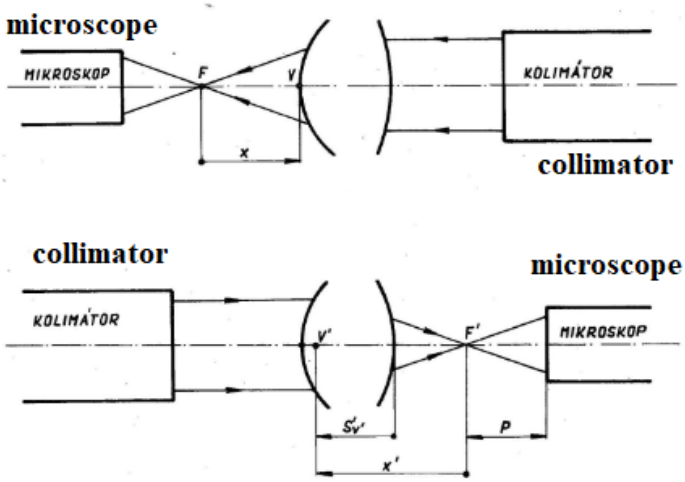

optical schematics of the experiment

Figure 5.9 collimatorr OSK

Measured values

PCX lens			
x_1 [mm]	x_1' [mm]	x_2 [mm]	x_2' [mm]
29.4	23.1	21.1	52.4

Newton's transfer equation is used:

$$x * x' = -f'^2 \tag{5-9}$$

Put values into this equation and the foci can be calculated $f' = 33.4\,mm$.
After measuring the data of the PCX lens, the distance of focal point from the last mechanical surface of the lens housing of the lens used as a collimator is measured: 39.5mm.

Because of the possible errors in the experiment and the limitation of the number of experiments, the focal length calculated based on the measured two sets of data is different.

5.2 Experimental structure

The schematic of the whole setup is shown in figure 5.10.

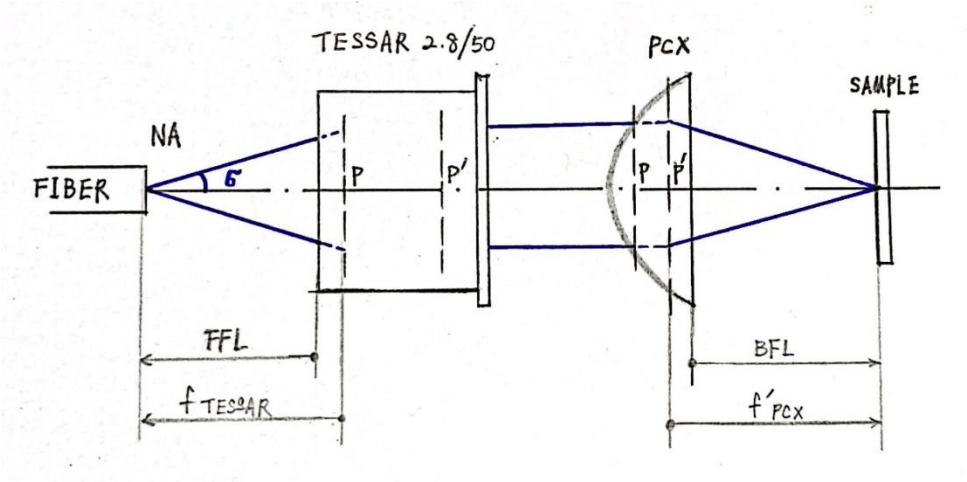

Figure 5.10 Schematic of the system

Experiment platform is shown as follows Figure 5.11. The tested object (mirror) is fixed on an micrometer-controlled XYZ stage.

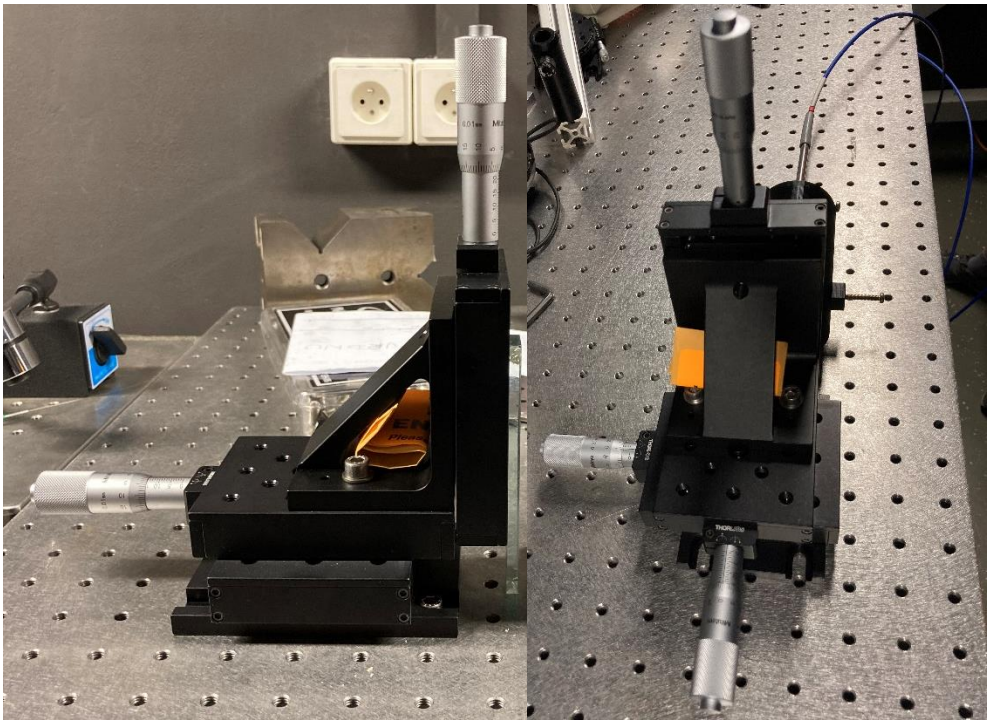

Figure 5.11 Experiment platform

We can use the three micrometers on the base to adjust the distance between the measured object and the lens. It can be seen from Figure 5.12 that a mirror is glued on the front of the board to act as the object to be measured. Fix the designed tube on the experimental platform and fix the sensor at its position.

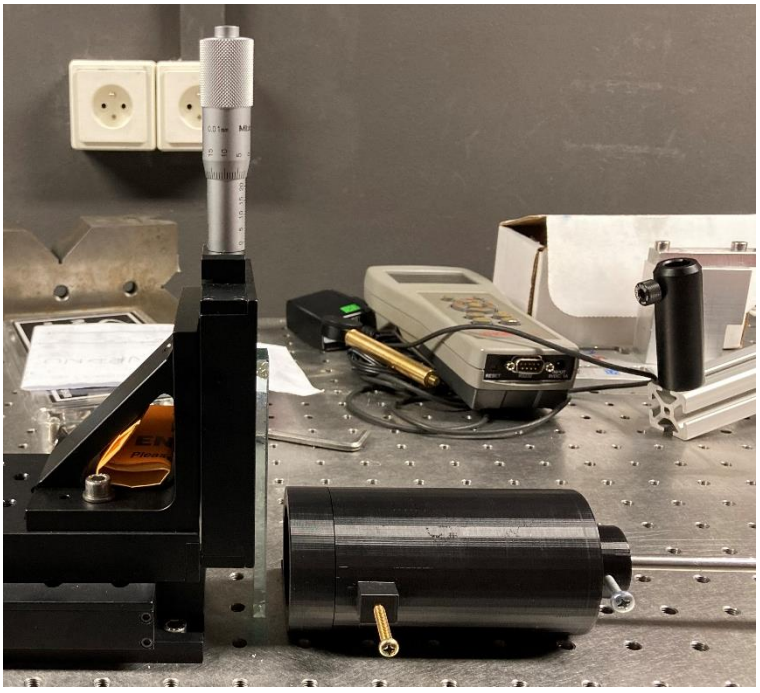

Figure 5.12 The entire experimental structure

Designed tube is shown in Figure 5.13.

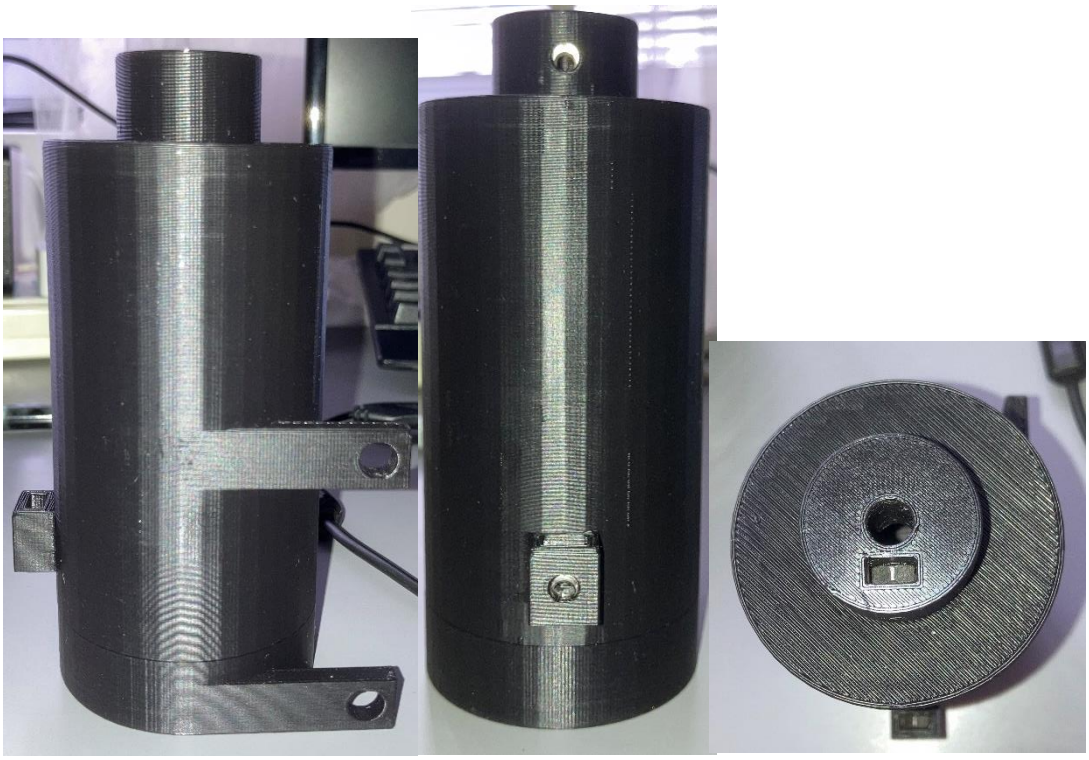

Figure 5.13 3D printed tube.

The placement of the two lenses inside the tube is shown in Figure 5.14. The two lenses fit tightly. Since light is incident from the focal point of the collimator, the light passing through the collimator is parallel light. The distance between the two lenses can take any value due to the parallel light. In order to save materials and time, the distance between them should be as small as possible.

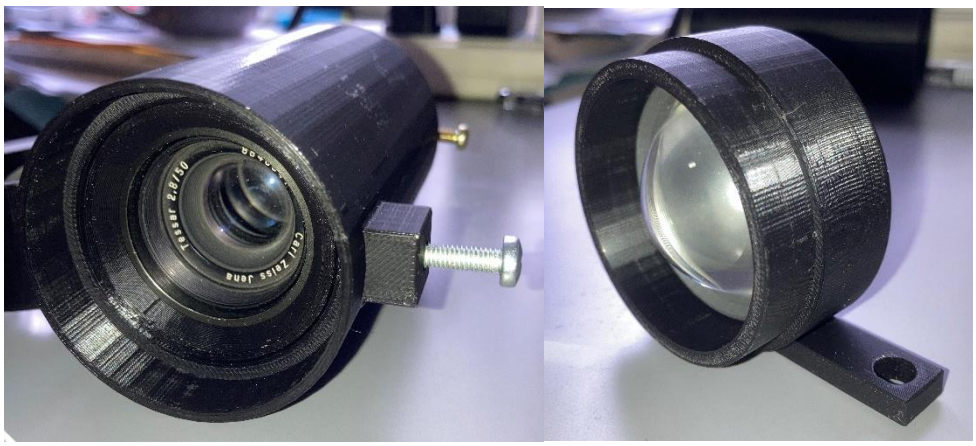

Figure 5.14 The structure of the tube and lenses' fixation.

Before fixing the sensor position, the focus of collimator is measured with a power meter shown in Figure 5.15.

Figure 5.15 Optical power meter THORLABS

Before connecting the system, the position of the fiber probe is measured with a power meter and OSK shown separately in Figure 5.15 and 5.9. We fixed the device with only lens used as collimator inside. We insert the fiber probe into its position which we measured in step 5.1.4 around 39.5 mm from the collimator and adjust the tightening of the screw so that the sensor head can move back and forth. There are two branches at the end of the sensor, one is connected to the light source and the other is connected to the optical power meter. When the sensor head moves back and forth, we can read the number from the power meter. When the reading reaches the maximum value, we tighten the screw. At this time, the fixed position of the sensor is the position where the sensor can sense the maximum amount of light. After measurement, the focal point is about 39mm in front of the collimator. When determining the fixed position of the sensor, the final experimental results can be more accurate. In addition, the experiment must be carried out in a dark place, because the reading of the power meter will change if the amount of light from outside enters the power meter, and the maximum value cannot be captured.

5.3 Experimental data processing

Start the experiment when all the components are connected. First adjust the position of the sensor to its focus, so that a very bright small spot can be seen while the reading on the computer reaches the maximum value. By controlling the micrometer, the distance between the center position of the dispersive focusing lens and the measured object is 7.5mm. Then add 0.5mm each time to know the 11mm position.

Record the data shown by the spectrometer each time. After finishing the measurement, organize the data and select the data of two different wavelengths to draw

a chart and analyze. Here I chose two wavelengths which are closed to the peak values, 720nm and 740nm. Establish the relationship between them and the displacement in turn. Direct data refers to the light intensity directly corresponding to each displacement. Because of the noise of light, the resulting graph is like jagged. But when we optimize the so-called zigzag chart using excel and control the wavelength between 700-750nm. For example, 11mm displacement measurement shown in figure 5.16.

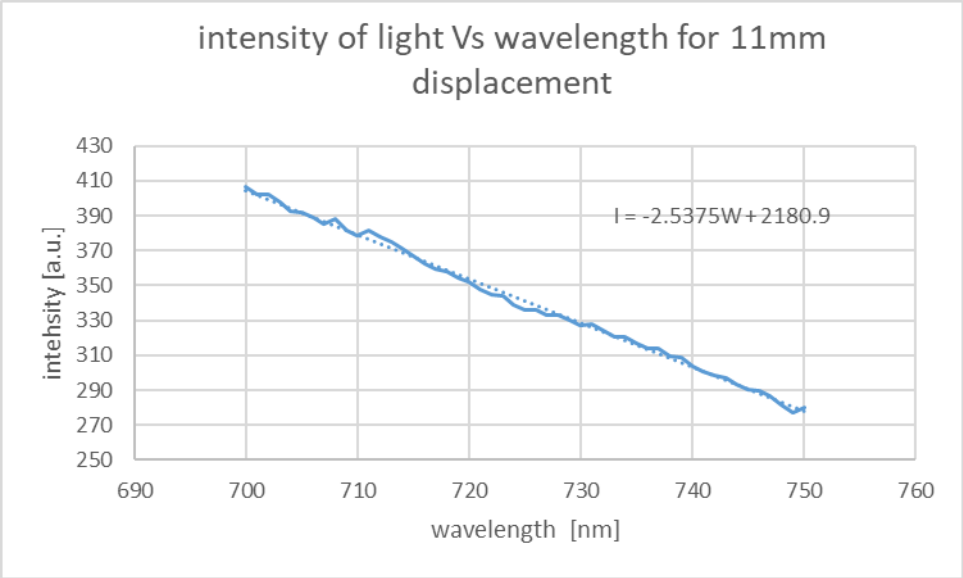

Figure 5.16 Intensity of light vs wavelength between 700-750nm at 11mm displacement.

From the graph after approximation, we can get a straight line that is the relationship between light intensity and wavelength. At the same time, its equation is displayed automatically by excel. After inserting the wavelength of 720 nm and 740 nm, we will get the calculated intensity for each other. These two kinds of data have been sorted and integrated into one chart.

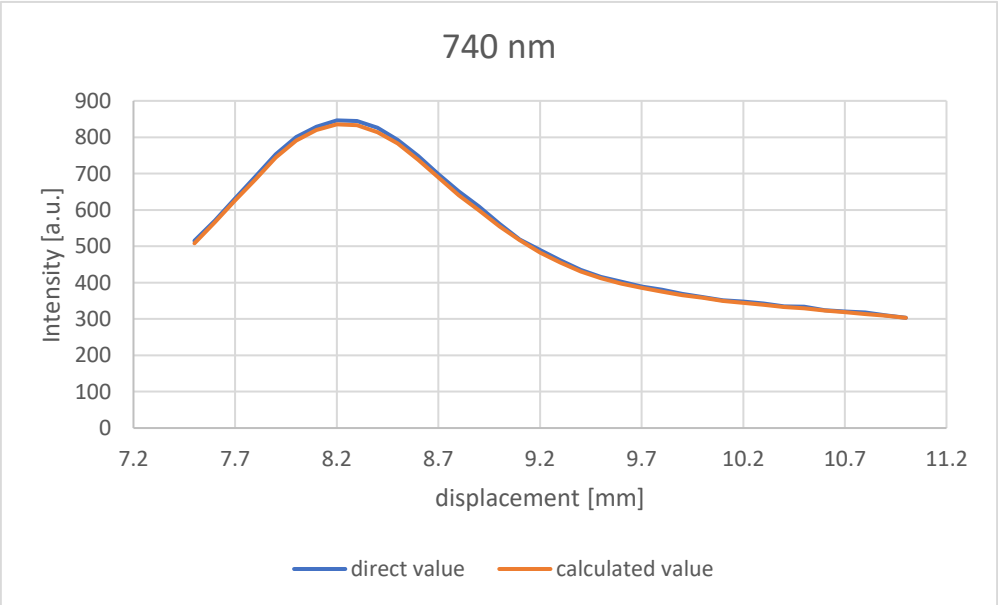

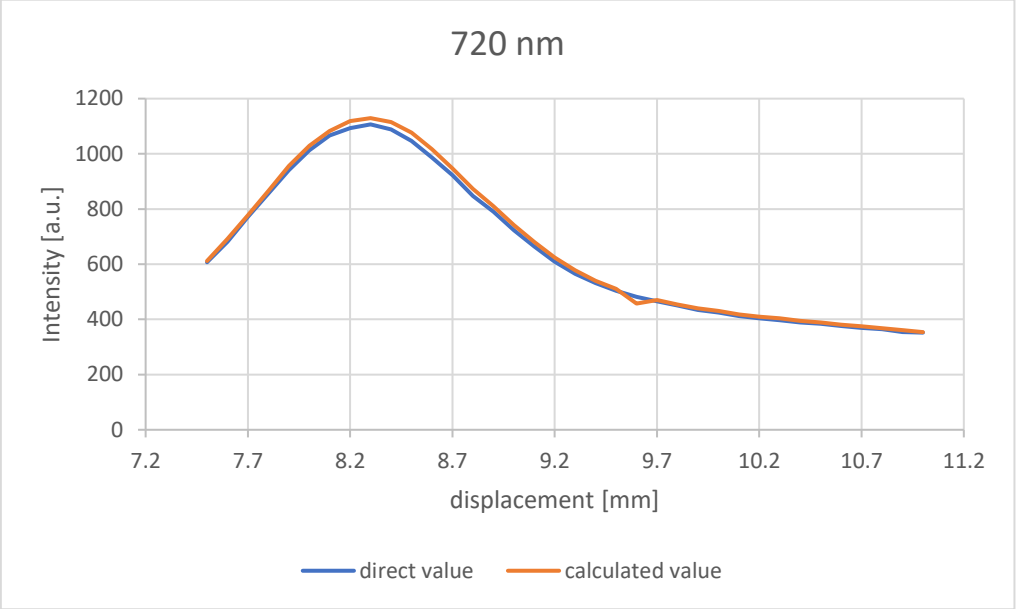

5.4 Light source spectrum analysis

Replace the previous experiment shown in step 5.3. We will use a different light source shown in figure 5.14. Mercury lamp has a line spectrum, we can observe the change in the intensity distribution for separate spectral lines when the tested object is moved along the optical axis.

Figure 5.14 Light source-Mercury lamp

The displacement is increased from 7.5mm to 11mm by 0.5mm each time to test and measure the corresponding light intensity.

After obtaining the experimental data, select four wavelengths of 404nm, 436nm, 546nm and 576nm (The wavelength corresponding to the maximum peak light intensity

obtained by comparing one by one) from the measurement to establish the relationship between their displacement and light intensity, as shown below.

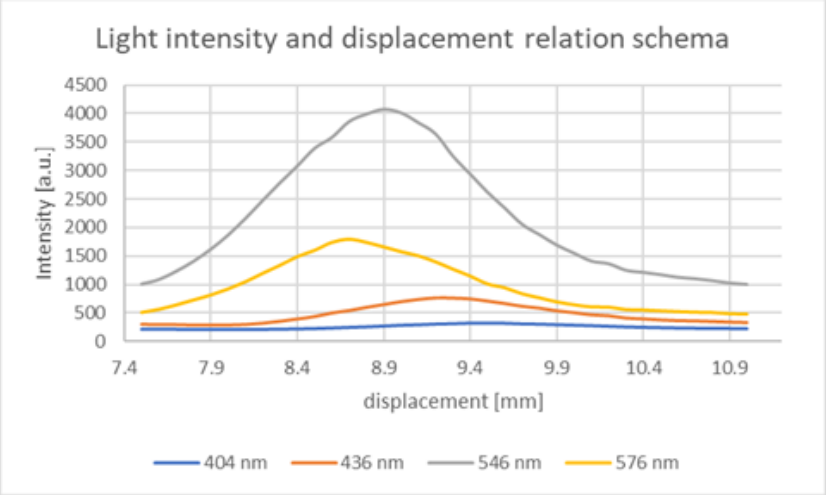

After dividing instantaneous intensity by the maximum intensity of light in each wavelength, the following diagram is obtained, and we can see the peak of the intensity changes with the object distance.

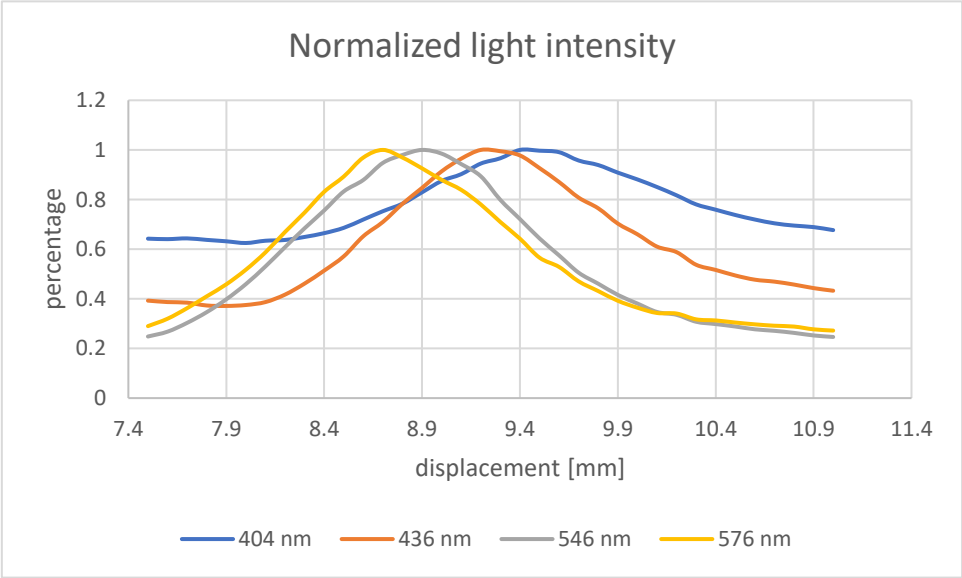

Then we easily find the displacement corresponding to the peaks of each curve and plot it versus wavelength.

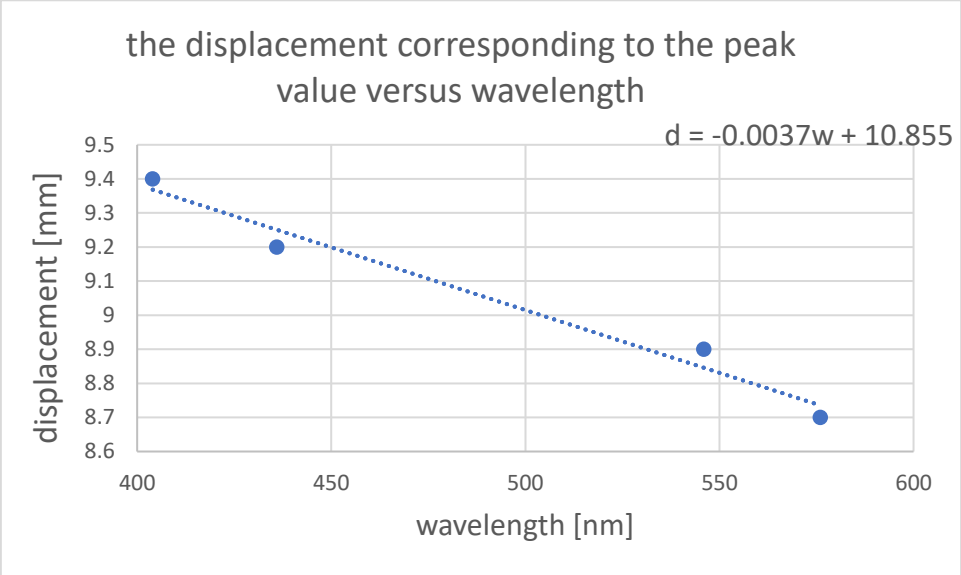

By approximating the resulting graph, we can find final curve is an approximate straight line.

$$d = -0.0037w + 10.855 \quad (5\text{-}10)$$

The sensitivity is -0.0037mm/nm or –3.7μm/nm.

Conclusion

The subject of the thesis analyzes and compares the characteristics of various types of displacement sensors. We develop a reasonable optical design to realize a chromatic confocal displacement sensor. The design of the dispersive objective lens was studied, and the color confocal optical experiment system was built to verify the feasibility of the design scheme and further experimental research was done. The specific work and results are divided into the following parts:

Theoretical analysis of the color confocal system, analyze the main parameters of the dispersive objective lens design, analyze the optical path principle of the commercial color confocal measurement system, and discuss the design content of dispersion and focus.

Build an experimental platform for the verification of the chromatic confocal principle to test the finished product parameters of the dispersive lens. Based on the dispersive lens design and experimental verification, a chromatic confocal measurement system is built. Detailed analysis of the optical path construction process.

Due to the small NA value, the experiment cannot accurately measure the state of the displacement of all wavelengths of light. When measuring the position where the sensor can receive the maximum light intensity, the power meter display data is too sensitive to find the best position, resulting in experimental error.

We found that the peak of light intensity always appears at the four wavelengths of 404nm, 436nm, 546nm and 576nm. We record the peak value measured after each displacement. After summarizing, it can be found that the maximum light intensity changes with the displacement. Because when selecting the peak value, the direct reading corresponding to the displacement is selected. However, because of the noise of light, the value selected in this way will either be higher or lower, which will bring uncertainty to the experimental results. The experimental results show the sensitivity of the experiment is –3.7μm/nm.

References

[1] Tao Renjun, Sun Zhongxin, Dong Liling. (2012). Analysis of Printed Board Warpage and Its Test Method.Printed. Circuit Information, 1, 56-60.

[2] Zeng Guanglong. (2006). Detection method of copper clad laminate and PCB warpage. Printed Circuit Information, 1, 52-55.

[3] Calculating Allowed Bow and Twist for Circuit Card Assemblies — Omnia MFG.(2021). [online] Available at: <https://www.omniamfg.com/mechanical/2020/10/9/calculating-allowed-bow-and-twist-for-circuit-card-assemblies> [Accessed 2 May 2021].

[4] The History and Basics of IPC Standards: The Official Standards for PCBs 2021. [online] Available at: <https://www.allaboutcircuits.com/news/ipc-standards-the-official-standards-for-pcbs/> [Accessed 2 May 2021].

[5] Variohm.com. 2021. Advantages of Non-Contact Linear Sensors. [online] Available at: <https://www.variohm.com/news-media/technical-blog-archive/advantages-of-non-contact-linear-sensors> [Accessed 2 May 2021].

[6] High-Accuracy Calibration Based on Linearity Adjustment for Eddy Current Displacement Sensor. (2021). [online] Available at: <https://www.mdpi.com/1424-8220/18/9/2842/htm> [Accessed 2 May 2021].

[7] conductor, C., 2021. Cause of skin effect: eddy current inside conductor. [online] Electrical Engineering Stack Exchange. Available at: <https://electronics.stackexchange.com/questions/242788/cause-of-skin-effect-eddy-current-inside-conductor> [Accessed 4 May 2021].

[8] Wang Hongbo. Research on the theory and design of sub-nanometer precision eddy current sensor[D]. Hefei: University of Science and Technology of China, 2015.

[9] Sensor Technology-Capacitive Sensor. (2021). [online] Available at: <https://blog.csdn.net/Ablities/article/details/114833658> [Accessed 4 May 2021].

[10] Capacitance - Wikipedia. (2021). [online] Available at: <https://en.wikipedia.org/wiki/Capacitance> [Accessed 5 May 2021].

[11] En.wikipedia.org. 2021. Scheimpflug principle - Wikipedia. [online] Available at: <https://en.wikipedia.org/wiki/Scheimpflug_principle> [Accessed 5 May 2021].

[12] Measurement principles of optical triangulation sensors. (2021). [online] Available at: <https://www.researchgate.net/figure/Measurement-principles-of-optical-triangulation-sensors_fig1_234972757> [Accessed 5 May 2021].

[13] 3D Reconstruction and Measurement of Surface Defects in Prefabricated Elements Using Point Clouds (2021). [online] Available at: <https://ascelibrary.org/doi/10.1061/%28ASCE%29CP.1943-5487.0000920> [Accessed 6 May 2021].

[14] profile, V. (2021). INTERFERENCE OF LIGHT. [online] Available at: <http://akarshansir.blogspot.com/2010/04/interference-of-light.html> [Accessed 6 May 2021].

[15] Wave Optics (2021). [online] Available at: <http://faculty.washington.edu/lylin/EE485W04/Ch2.pdf> [Accessed 6 May 2021].

[16] En.wikipedia.org. 2021. White light interferometry - Wikipedia. [online] Available at: <https://en.wikipedia.org/wiki/White_light_interferometry> [Accessed 7 May 2021].

[17] Diva-portal.org. 2021. [online] Available at: <https://www.diva-portal.org/smash/get/diva2:395542/FULLTEXT01.pdf> [Accessed 7 May 2021].

[18] Principles of interference microscopy for the measurement of surface topography (2021). Retrieved 15 May 2021, [online] Available at: <https://www.osapublishing.org/aop/abstract.cfm?URI=aop-7-1-1> [Accessed 12 May 2021].

[19] (2021) Film thickness measurement based on nonlinear phase analysis using a Linnik microscopic white-light spectral interferometer. [online] Available at: <https://www.osapublishing.org/ao/abstract.cfm?uri=ao-57-12-2955> [Accessed 12 May 2021].

[20] Drayton, B. Algorithm and design improvements for indirect time of flight range imaging cameras. 2013.

[21] En.wikipedia.org. 2021. A Time-of-Flight Range Sensor Using Four-Tap Lock-In Pixels with High near Infrared Sensitivity for LiDAR Applications. [online] Available at: <https://www.mdpi.com/1424-8220/20/1/116/htm> [Accessed 15 May 2021].

[22] zhihu. 2021. Principles and differences between DTOF and ITOF. [online] Available at: <https://zhuanlan.zhihu.com/p/195055006> [Accessed 15 May 2021].

[23] Drayton, B., 2021. Algorithm and design improvements for indirect time of flight

range imaging cameras. [online] Researcharchive.vuw.ac.nz. Available at: <https://researcharchive.vuw.ac.nz/xmlui/handle/10063/2895> [Accessed 12 May 2021].

[24] Direct time-of-flight (D-TOF) image sensor for LiDAR applications. (2021). [online] Available at: <https://www.epfl.ch/labs/aqua/research/lidar/tof-lidar/> [Accessed 16 May 2021].

[25] Structure design and simulation analysis of inductive displacement sensor (2021). [online] Available at: <https://www.semanticscholar.org/paper/Structure-design-and-simulation-analysis-of-sensor-Rui-Hongwei/fcc8e80cc4673f0863ef107262399503176bcc09> [Accessed 19 May 2021].

[26] What is the principle of a current transformer? What are the wiring forms. (2021). [online] Available at: <https://zhuanlan.zhihu.com/p/51170598> [Accessed 19 May 2021].

[27] Eurekamagazine.co.uk. 2021. Factors to consider when selecting confocal displacement sensors. [online] Available at: <https://www.eurekamagazine.co.uk/design-engineering-features/technology/factors-to-consider-when-selecting-confocal-displacement-sensors/174617/> [Accessed 20 May 2021].

[28] CCMP2. (2021). [online] Available at:< https://www.trimos.com/optical-measurement/technologies/technology-ccmp2> [Accessed 20 May 2021].

[29] Euspen.eu. 2021. [online] Available at: <https://www.euspen.eu/knowledge-base/ICE10242.pdf> [Accessed 20 May 2021].

[30] Fiber Optic Displacement Sensors and Their Applications. 2021. [online] Available at: <https://www.researchgate.net/publication/221925344_Fiber_Optic_Displacement_Sensors_and_Their_Applications> [Accessed 20 May 2021].

[31] Fibre optic displacement sensor for the measurement of amplitude and frequency of vibration. 2021. [online] Available at: <https://www.sciencedirect.com/science/article/abs/pii/S0030399207000035> [Accessed 20 May 2021].

[32] Slidetodoc.com. 2021. UNITV PHOTONICS AND FIBRE OPTICS Basics of laser. [online] Available at: <https://slidetodoc.com/unitv-photonics-and-fibre-optics-basics-of-laser/> [Accessed 20 May 2021].

[33] Krohn, D., MacDougall, T. and Méndez, A., n.d. Fiber optic sensors ISBN:

9781628411805.

[34] Efunda.com. 2021. eFunda: Theory of Fiber Optic Sensors. [online] Available at: <https://www.efunda.com/DesignStandards/sensors/fotonic/fotonic_theory.cfm> [Accessed 24 May 2021].

[35] Krohn, D., MacDougall, T. and Méndez, A., n.d. Fiber optic sensors ISBN: 9781628411805.

[36] Corning.com. 2021. [online] Available at: <https://www.corning.com/media/worldwide/coc/documents/Fiber/white-paper/WP1212.pdf> [Accessed 26 May 2021].

[37] Hindawi.com. 2021. Figure 4 | Vibration Detection Using Optical Fiber Sensors. [online] Available at: <https://www.hindawi.com/journals/js/2010/936487/fig4/> [Accessed 26 May 2021].

[38] Fiber Bragg Grating Displacement Sensor with High Abrasion Resistance for a Steel Spring Floating Slab Damping Track. 2021. [online] Available at: <https://www.mdpi.com/1424-8220/18/6/1899> [Accessed 26 May 2021].

[39] Krohn, D., MacDougall, T. and Méndez, A., n.d. Fiber optic sensors ISBN: 9781628411805.

[40] Schematic diagram of an FBG sensor. 2021. [online] Available at: <https://www.researchgate.net/figure/Schematic-diagram-of-an-FBG-sensor-a-principle-of-the-FBG-sensor-b-wavelength-shift_fig2_318519996> [Accessed 28 May 2021].

[41] Wide Range FBG Displacement Sensor Based on Twin-Core Fiber Filter. 2021. [online] Available at: <https://www.semanticscholar.org/paper/Wide-Range-FBG-Displacement-Sensor-Based-on-Fiber-Zou-Dong/f4a82efd73af879be83f7e5b559dd81fb94effbe> [Accessed 28 May 2021].

[42] Micro-epsilon.com. 2021. [online] Available at: <https://www.micro-epsilon.com/download/products/cat--eddyNCDT--en.pdf> [Accessed 29 May 2021].

[43] Micro-epsilon.com. 2021. [online] Available at: <https://www.micro-epsilon.com/download/products/cat--capaNCDT--en.pdf> [Accessed 29 May 2021].

[44] Micro-epsilon.com. 2021. [online] Available at: <https://www.micro-epsilon.com/download/products/cat--optoNCDT--en.pdf> [Accessed 29 May 2021].

[45] Micro-epsilon.com. 2021. [online] Available at: <https://www.micro-

epsilon.com/download/products/cat--confocalDT--en.pdf> [Accessed 29 May 2021].

[46] Keyence.eu. 2021. Confocal Displacement Sensor - CL-3000 series | KEYENCE International Belgium. [online] Available at: <https://www.keyence.eu/products/measure/laser-1d/cl-3000/> [Accessed 29 May 2021].

[47] Micro-epsilon.com. 2021. [online] Available at: <https://www.micro-epsilon.com/download/products/cat--interferoMETER--en.pdf> [Accessed 30 August 2021].

[48] Micro-epsilon.com. 2021. [online] Available at: <https://www.micro-epsilon.com/download/products/cat--optoNCDT-ILR--en.pdf> [Accessed 30 May 2021].

[49] Micro-epsilon.com. 2021. [online] Available at: <https://www.micro-epsilon.com/download/products/cat--induSENSOR--en.pdf> [Accessed 30 May 2021].

[50] qmt. 2021. Confocal Chromatic. [online] Available at: <https://www.qmt-group.com/event/307/technologies/confocal-chromatic/> [Accessed 30 May 2021].

[51] Luo Chunhua, Mou Da, Li Yanhong . Optical Design and ZEMAX Applications [M]. Changchun University of Technology, 2013.

[52] Oceaninsight.com. 2021. Fibers & probes | Spectroscopy | Ocean Insight. [online] Available at: <https://www.oceaninsight.com/products/fibers-and-probes/> [Accessed 31 May 2021].

[53] Kullabs.com. 2021. Chromatic Aberrations in Lenses | Notes, Videos, QA and Tests | Grade 11>Physics>Dispersion of Light | Kullabs. [online] Available at: <https://kullabs.com/class-11/physics-11/dispersion-of-light/chromatic-aberrations-in-lenses> [Accessed 31 May 2021].

[54] Eckop.com. 2021. Numerical Aperture and F-Number - Eckhardt Optics - Equating to f/#. [online] Available at: <https://www.eckop.com/resources/optics/numerical-aperture-and-f-number/> [Accessed 31 May 2021].

[55] En.wikipedia.org. 2021. Numerical aperture - Wikipedia. [online] Available at: <https://en.wikipedia.org/wiki/Numerical_aperture> [Accessed 31 May 2021]

Appendix

Models of all the sensors mentioned above.

Type	Model	Measuring range [mm]	Linearity [µm]	Resolution [µm]	Operating temperature [°C]
Eddy Current displacement sensors [42]					
Eddy NCDT 3001	DT3001-U2-A-SA/DT3001-U2-M-SA	2	< ±28	4	0 … +70
	DT3001-U4-A-SA/U4-M-SA/U4-A-Cx/U4-M-Cx	4	< ±28	4	
	DT3001-U6-A-SA/U6-M-SA	6	< ±15	3	-20 … +70
	DT3001-U8-A-SA/U8-M-SA	8	< ±20	4	
Eddy NCDT 3005	DT3005-U1-A-C1/U1-M-C1	1	< ±2.5	0.5	-20 … +125 (Optional -20... +180)
	DT3005-S2-A-C1/S2-M-C1	2	< ±5	1	
	DT3005-U3-A-C1/U3-M-C1	3	< ±7.5	1.5	
	DT3005-U6-A-C1/U6-M-	6	< ±15	3	

	C1				
Eddy NCDT 3060	ES-U1	1	< ±1	0.02	-20 … +180
	ES-S1	1	< ±1	0.02	
	ES-U2	2	< ±2	0.04	-20 … +200
	ES-S2	2	< ±2	0.04	
	ES-U3	3	< ±3	0.06	
	ES-S4	4	< ±4	0.08	
	ES-U6	6	< ±6	0.12	
	ES-U8	8	< ±8	0.16	
Eddy NCDT 3070	ES-S04	0.4	< ±1	0.02	0 … +180
Eddy NCDT 3300	ES04	0.4	< ±0.8	0.04	0 ... +150
	EU05	0.4	< ±1	0.05	
	ES08	0.8	< ±1.6	0.04	
	ES1	1	< ±2	0.05	
	EU1	1	< ±2	0.05	-40 … +150
	ES2	2	< ±4	0.1	-20 … +150
	EU3	3	< ±6	0.15	
	ES4	4	< ±8	0.2	0 … +150
	EU6	6	< ±12	0.3	-20 … +150
	EU8	8	< ±16	0.4	0 … +150
	EU15	15	< ±30	0.75	
	EU22	22	< ±44	1.1	
	EU40	40	< ±80	2	
Eddy NCDT SGS4701	SGS4701	0.5	< ±2	0.5	+10 … +80
EX-V Series	EX-305V	1	±0.3% of F.S.	0.4	-10 … +60
	EX-110V	2		0.4	
	EX-416V	5		1	
	EX-422V	10		2	
	EX-614V	4		1	
Capacitive displacement sensor [43]					
Capa NCDT Cylindrical sensors with female connect	CS005	0.05	≤ ±0.15	static 2Hz: 0.000037	-50 … +200
				Dynamic 8.5KHz: 0.001	
	CS02	0.2	≤ ±0.4	static 2Hz: 0.00015	
				Dynamic 8.5KHz: 0.004	

or	CS05	0.5	≤ ±0.15	static 2Hz: 0.000375	
				Dynamic 8.5KHz: 0.01	
	CSE05	0.5	≤ ±0.5	static 2Hz: 0.000375	
				Dynamic 8.5KHz: 0.01	
	CS08	0.8	≤ ±0.4	static 2Hz: 0.0006	
				Dynamic 8.5KHz: 0.016	
	CS1	1	≤ ±1.5	static 2Hz: 0.00075	
				Dynamic 8.5KHz: 0.02	
	CS1HP	1	≤ ±1.5	static 2Hz: 0.00075	
				Dynamic 8.5KHz: 0.02	
	CSE1	1	≤ ±1	static 2Hz: 0.00075	
				Dynamic 8.5KHz: 0.02	
	CSE1,25	1.25	≤ ±1.25	static 2Hz: 0.0009	
				Dynamic 8.5KHz: 0.025	
	CS2	2	≤ ±1	static 2Hz: 0.0015	
				Dynamic 8.5KHz: 0.04	
	CSE2	2	≤ ±2	static 2Hz: 0.0015	
				Dynamic 8.5KHz: 0.04	
	CS3	3	≤ ±0.9	static 2Hz: 0.00225	
				Dynamic 8.5KHz: 0.06	
	CSE3	3	≤ ±3	static 2Hz: 0.00225	
				Dynamic 8.5KHz: 0.06	
	CS5	5	≤ ±2.5	static 2Hz: 0.00375	
				Dynamic 8.5KHz:	

				0.1	
	CS10	10	≤ ±15	static 2Hz: 0.9	
				Dynamic 8.5KHz: 24	
Cylindrical sensors with thread and socket	CSE05/M8	0.5	≤ ±0.5	static 2Hz: 0.000375	-50 … +200
				Dynamic 8.5KHz: 0.01	
	CSE1,25/M12	1.25	≤ ±1.25	static 2Hz: 0.00095	
				Dynamic 8.5KHz: 0.025	
	CSE2/M16	2	≤ ±2	static 2Hz: 0.0015	
				Dynamic 8.5KHz: 0.04	
	CSE3/M24	3	≤ ±3	static 2Hz: 0.00225	
				Dynamic 8.5KHz: 0.06	
Cylindrical sensors with integrated cable	CSH02-CAm1,4	0.2	≤ ±0.054	static 2Hz: 0.00015	-50…+200
				Dynamic 8.5KHz: 0.004	
	CSH05-CAm1,4	0.5	≤ ±0.13	static 2Hz: 0.00038	
				Dynamic 8.5KHz: 0.01	
	CSH1-CAm1,4	1	≤ ±0.13	static 2Hz: 0.00075	
				Dynamic 8.5KHz: 0.02	
	CSH1,2-CAm1,4	1.2	≤ ±0.84	static 2Hz: 0.0009	
				Dynamic 8.5KHz: 0.024	
	CSH2-CAm1,4	2	≤ ±0.5	static 2Hz: 0.0015	
				Dynamic 8.5KHz: 0.04	
Flat sensors with connector	CSG0,50-CAm2,0	0.5	≤ ±0.5	static 2Hz: 0.004	-50 … +100
				Dynamic 8.5KHz: 0.18	
	CSG1,00-CAm2,0	1	≤ ±1	static 2Hz: 0.008	
				Dynamic 8.5KHz: 24	

Flat sensors with integrated cable	CSH02FL-CRm1,4	0.2	≤ ±0.05	static 2Hz: 0.00015	-50 … +200
				Dynamic 8.5KHz: 0.004	
	CSH05FL-CRm1,4	0.5	≤ ±0.09	static 2Hz: 0.00038	
				Dynamic 8.5KHz: 0.01	
	CSH1FL-CRm1,4	1	≤ ±0.2	static 2Hz: 0.00075	
				Dynamic 8.5KHz: 0.02	
	CSH1,2FL-CRm1,4	1.2	0.84	static 2Hz: 0.0009	
				Dynamic 8.5KHz: 0.024	
	CSH2FL-CRm1,4	2	0.32	static 2Hz: 0.0015	
				Dynamic 8.5KHz: 0.04	
	CSH3FL-CRm1,4	3	≤±0.9	static 2Hz: 0.00225	
				Dynamic 8.5KHz: 0.06	
Triangulation displacement sensor [44]					
optoNCDT 1220	ILD1220-10	10	< ±10	1	0 ... +50
	ILD1220-25	25	< ±25	2.5	
	ILD1220-50	50	< ±50	5	
optoNCDT 1320	ILD1320-10	10	< ±10	1	0 ... +50
	ILD1320-25	25	< ±25	2.5	
	ILD1320-50	50	< ±50	5	
optoNCDT 1420	ILD1420-10	10	< ±8	0.5	0 ... +50
	ILD1420-25	25	< ±20	1	
	ILD1420-50	50	< ±40	2	
optoNCDT	ILD1420-10CL1	10	< ±8	0.5	0 ... +50

1420 CL1	ILD1420-25CL1	25	< ±20	1	
	ILD1420-50CL1	50	< ±40	2	
optoNCDT 1750	ILD1750-2	2	< ±1.6	0.1	0 ... +50
	ILD1750-10	10	< ±6	0.4	
	ILD1750-20	20	< ±12	0.8	
optoNCDT 1900	ILD1900-2	2	< ±1	< 0.1	0 ... +50
	ILD1900-10	10	< ±2	< 0.4	
	ILD1900-25	25	< ±5	< 0.8	
optoNCDT 2300	ILD2300-2	2(2) Value in brackets is for a measuring rate of 49.14 kHz	< ±0.6	0.03	0 ... +50
	ILD2300-5	5(2)	< ±1.5	0.08	
	ILD2300-10	10(5)	< ±2	0.15	
	ILD2300-20	20(10)	< ±4	0.3	
	ILD2300-50	50(25)	< ±10	0.8	
optoNCDT 1750LL	ILD1750-2LL	2	< ±1.6	0.1	0 ... +50
	ILD1750-10LL	10	< ±6	0.4	
	ILD1750-20LL	20	< ±12	0.8	
	ILD1750-50LL	50	< ±30	2	
optoNCDT 1900LL	ILD1900-2LL	2	< ±1	< 0.1	0 ... +50
	ILD1900-10LL	10	< ±2	< 0.4	
	ILD1900-25LL	25	< ±5	< 0.8	
optoNC	ILD2300-	2(2)	< ±0.6	0.03	0 ... +50

DT 2300LL	2LL				
	ILD2300-10LL	10(5)	< ±2	0.15	
	ILD2300-20LL	20(10)	< ±4	0.3	
optoNCDT 2300BL	ILD2300-2BL	2(2)	< ±0.6	0.03	0 ... +50
	ILD2300-5BL	5(2)	< ±1.5	0.08	
	ILD2300-10BL	10(5)	< ±2	0.15	
optoNCDT 1750DR	ILD1750-2DR	2	< ±1.6	0.1	0 ... +50
	ILD1750-10DR	10	< ±6	0.4	
optoNCDT 2300-2DR	ILD2300-2DR	2(1)	< ±0.6	0.03	0 ... +50
Chromatic confocal displacement sensor [45][46]					
confocalDT IFS2402	IFS2402-0,4	0.4	< ±0.3	static: 0.016	+5 … +70
				dynamic: 0.048	
	IFS2402-1.5	1.5	< ±1.5	static: 0.06	
				dynamic: 0.192	
	IFS2402-4	3.5	< ±3	static: 0.1	
				dynamic: 0.48	
	IFS2402/90-1,5	1.5	< ±1.2	static: 0.06	
				dynamic: 0.192	
	IFS2402/90-4	2.5	< ±3	static: 0.1	
				dynamic: 0.48	
confocalDT IFS2403	IFS2403-0.4	0.4	< ±0.3	static: 0.016	+5 … +70
				dynamic: 0.047	
	IFS2403-1.5	1.5	< ±1.2	static: 0.06	
				dynamic: 0.186	
	IFS2403-4	4	< ±3	static: 0.1	
				dynamic: 0.46	
	IFS2403-10	10	< ±20	static: 0.25	
				dynamic: 1.25	
	IFS2403/90-1.5	1.5	< ±1.2	static: 0.06	
				dynamic: 0.186	
	IFS2403/90-4	4	< ±3	static: 0.1	
				dynamic: 0.46	
	IFS2403/9	10	< ±20	static: 0.25	

	0-10			dynamic:1.25	
confocalDT IFS2404	IFS2404-2	2	< ±1	static: 0.04	+5 … +70
				dynamic: 0.125	
	IFS2404/90-2	2	< ±1	static: 0.04	
				dynamic: 0.125	
confocalDT IFS2405	IFS2405-0.3	0.3	< ±0.15	static: 0.004	+5 … +70
				dynamic: 0.02	
	IFS2405-1	1	< ±0.25	static: 0.028	
				dynamic: 0.052	
	IFS2405-3	3	< ±0.75	static: 0.06	
				dynamic: 0.126	
CL-3000 Series	CL-L007	1.5	±2.1	0.25	0 … +50
	CL-L015	1.3	±0.49		
	CL-L030	3.7	±0.94		
	CL-P007	1.5	±0.96		
	CL-P015	1.3	±0.49		
	CL-P030	3.7	±0.94		
LK-G5000 Series	LK-H008W	0.5	±0.5	0.005	0 … +50
	LK-H025	3	±1.2	0.002	
	LK-H027	3			
	LK-H008	0.5	±0.5	0.005	
	LK-H020	3	±1.2	0.002	
	LK-H022	3			
	LK-H008	0.5	±0.5	0.005	
	LK-H008W	0.5			
	LK-H022K	2.8	±1.2	0.002	
	LK-H027K	2.8			
Interferometers [47]					
interferoMETER 5400-DS	IMS5400-DS	2.1	< ±50	< 0.001	+5 … +70
interferoMETER 5400-	IMS5400-TH45	0.035 … 1.4	< ±0.1	< 0.001	+5 … +70
	IMS5400-TH70		< ±0.2		

TH					
interferoMETER 5600-DS	IMS5600-DS	2.1	< ±0.01	$< 3.0\times10^{-5}$	+5 … +70
Laser distance sensors (time-of-flight) [48]					
optoNCDT ILR 103x/LC1	ILR1030-8/LC1	Black 10%: 200 … 2500	< ±20000	1000	-30 … +55
		Gray 18%: 200 … 3500			
		White 90%: 200 … 2500			
		Reflector: -			
	ILR1030-15/LC1	Black 10%: 200 … 5000			
		Gray 18%: 200 … 6000			
		White 90%: 200 … 15000			
		Reflector: -			
	ILR1031-50/LC1	Black 10%: -			
		Gray 18%: -			
		White 90%: -			
		Reflector: 200 … 50000			
optoNCDT ILR 118x-30	ILR1182-30	Black 10%: 400 … 17000 Gray 18%: 100 … 30000 White 90%: 100 … 50000 Reflector: 50000-150000	< ±200 (+15 … +30); <±500 (- 40 … +55)	100	-10 … + 55
	ILR1183-30				
Inductive displacement sensor [49]					
induSENSOR DTA (LVDT)	DTA-1G8	±1	≤ ±3	≤0.15	-20 …+80 (without bellows); 0 … 80 (with bellows)
	DTA-3G8	±3	≤ ±9	≤0.45	
	DTA-5G8	±5	≤ ±15	≤0.75	

	DTA-10G8	±10	≤ ±30	≤1.5	
	DTA-1G8-V	±1	≤ ±3	≤0.15	
	DTA-3G8-V	±3	≤ ±9	≤0.45	
	DTA-5G8-V	±5	≤ ±15	≤0.75	
	DTA-10G8-V	±10	≤ ±30	≤1.5	

Technical drawings of designed tubes and lenses' fixation.